

THESIS FOR THE DEGREE OF DOCTOR OF PHILOSOPHY

Experimental Study on Truck Related Power
Losses: The Churning Losses in a Transmission
Model and Active Flow Control at an A-pillar of
Generic Truck Cabin Model

Erwin Adi Hartono



Department of Mechanics and Maritime Sciences
CHALMERS UNIVERSITY OF TECHNOLOGY
Göteborg, Sweden 2019

Experimental Study on Truck Related Power Losses: The Churning Losses in a
Transmission Model and Active Flow Control at an A-pillar of Generic Truck Cabin
Model

ERWIN ADI HARTONO
ISBN 978-91-7597-844-4

© ERWIN ADI HARTONO, 2019.

Doktorsavhandlingar vid Chalmers tekniska högskola
Ny serie nr 4525
ISSN 0346-718X

Department of Mechanics and Maritime Sciences
Chalmers University of Technology
SE-412 96 Göteborg, Sweden
Telephone + 46 (0) 31 – 772 1000

Typeset by the author using L^AT_EX.

Printed by Chalmers Reproservice
Göteborg, Sweden 2019

Perfect is the enemy of good.

- Voltaire

Abstract

The fight with global warming constantly forces vehicle manufacturers to innovate, in order to reduce the CO₂ emissions of their products. This means that marginal efficiency gains in every component are considered beneficial for total reduction of CO₂ emissions. For long-haul heavy-duty trucks, the transmission losses and the aerodynamic drag are two of the most important losses.

If we look at truck transmission, losses in the form of churning losses stem from the interaction between oil and partially immersed rotating gear wheels. It is obvious that reducing the amount of oil inside the transmission will lower the churning losses. However, the presence of oil inside a transmission is not solely for lubrication purposes but also for heat dissipation. Excessive heat on the components greatly impacts their durability/lifetime. Finding a balance between low loss and high heat dissipation requires further studies in the area of fluid dynamics.

In this study, oil flow inside a transmission was studied by means of flow visualisation, velocity measurement, and torque measurement. A simplified version of a transmission was specially built to allow the oil flow inside the gearbox to be studied in more detail. The test section, test object, and test oil have a clear appearance in order to ensure good optical access. Flash photography and high speed recording were used to visually capture the oil flow. Particle image velocimetry was used to measure the oil flow velocity. The torque loss was measured for different oil levels and gear geometries. The torque loss estimation formula was fitted with the help of a machine learning algorithm in the search for a general equation that described the churning losses.

The results show that rotational speed, immersion depth and geometry have significant effects on splash pattern and oil distribution inside the transmission. The 2C2D-PIV measured the oil flow velocity in the mid-plane and revealed recirculation regions below the gear and the pinion. The 3C2D-PIV was done in several different planes and reconstruction of the data shows the three-dimensional flow below the gear wheel. Cross-plane measurement revealed vortices below the gear wheel and oil flow velocity in the gear meshing region. Air entrainment into the oil sump (aeration) was observed during the measurement. Aeration was caused by solid and liquid impingement on the free surface. The aeration level was estimated to be up to 20%. Torque measurement showed up to a 9% increase in torque when comparing torque data between aerated and non-aerated oil. Curve fitting to the torque measurement data was done with the help of a machine learning algorithm.

If we look at the truck aerodynamics drag, it stems from flow separation. Trucks are considered as bluff bodies from a fluid dynamics perspective. The aerodynamic drag of a bluff body is dominated by the pressure drag, which is the pressure difference between the stagnation point and the wake. The earlier the flow separates from the

body, the larger the wake size. There are several locations in the truck where the flow separates: the front of the truck; the A-pillar; the under-body and the wheel; the gap between tractor and trailer; and the wake behind the trailer.

In this study, flow separation at the A-pillar was investigated. An active flow control in terms of zero net flux synthetic jets was applied. The role of the synthetic jets was to energise the boundary layer, which in turn suppressed the flow separation. The study was performed in a generic truck cabin model built specially for this study. The measurements were done at Chalmers wind tunnel with an inlet velocity of 20 m/s . Combining the inlet speed with the 0.4 m characteristic length of the model, the resulting Reynolds number was 5×10^5 . Pressure measurement and velocity measurement were done using time-resolved PIV to quantify the flow velocity field with and without the active flow control at the side and at the wake region of the test object. Four different actuation cases ($F^+ = 1, 2.1, 3.1, \text{ and } 6.2$) of the synthetic jet were studied and measured. Hot wire anemometry was used to characterise the actuators that produced the synthetic jet.

The results suggest that the receptive band of the shear layer and wake in this study was located in the range between $0.7 < F^+ < 3.1$. The chosen F^+ values of 1, 2.1, 3.1, and 6.2 successfully showed suppression of the flow separation at the A-pillar. The $F^+ = 1$ showed the lowest absolute streamwise velocity and the shortest wake. The $F^+ = 2.1$ and 3.1 showed a lower base pressure region and a very similar wake configuration. The strongest level of flow separation suppression occurred at $F^+ = 3.1$. The $F^+ = 6.2$ was chosen to confirm the previous study's finding that the velocity fields in the wake are independent of actuation frequency.

The experimental data gathered in this study was proven to be useful and was used to validate a numerical simulation. The experimental data from the churning losses study was used to validate a numerical method, smoothed particle hydrodynamics. The data from the active flow control study was used to validate a CFD simulation using a PANS turbulence model. Through these experiments, additional knowledge was contributed to the fields of fluid dynamics, especially in the area of oil flow around a spur gear inside a transmission and active flow control using synthetic jets for A-pillars. The work has laid a good foundation for future study on these topics.

Keywords: Gearbox, Transmission, Load independent power losses, Churning losses, Aeration, Flow separation, A-Pillar, Active Flow Control, Synthetic Jets, Particle Image Velocimetry, Hot wire anemometry, Torque measurement, Flow visualization, Curve fit, Machine learning, CFD, SPH, Computational Fluid Dynamics, Smoothed Particle Hydrodynamics.

Acknowledgments

I was planning to write all your names and acknowledge all your contributions. However, after some thinking, I decided not to due to the General Data Protection Regulation. Joking aside, it was because my list became so long and personal. So, I decided to include only the names of the institutions you belong to. Every one of you had your own unique role in my PhD journey and for that I thank you sincerely.

Here is the list of institutions in alphabetical order:

- Chalmers University of Technology
- FluidDyna Gmbh
- Institute of Thermophysics SB RAS
- KTH Royal Institute of Technology
- Novosibirisk State University
- Vicura AB
- VINNOVA
- Volvo Powertrain AB

Another list containing special people outside my professional world:

- My parents
- My wife
- My daughter
- My friends

Erwin Adi Hartono
Göteborg, January 2019

List of Publications

This thesis is based on the following appended papers below. The division of work can be found in chapter 4

Paper 1. Erwin Adi Hartono, Maxim Golubev, and Valery Chernoray. *PIV Study of Fluid Flow Inside a Gearbox*. Proceedings of the 10th International Symposium on Particle Image Velocimetry. Delft, The Netherlands, July 1-3, 2013.

Paper 2. Erwin Adi Hartono, Alexandr Pavlenko, and Valery Chernoray. *Stereo-PIV Study of Oil Flow Inside a Model Gearbox*. Proceedings of 17th International Symposium on Applications of Laser Techniques to Fluid Mechanics. Lisbon, Portugal, 07-10 July, 2014.

Paper 3. Zhe Ji, Miloš Stanić, Erwin Adi Hartono, and Valery Chernoray. *Numerical simulations of oil flow inside a gearbox by Smoothed Particle Hydrodynamics (SPH) method*. Tribology International 127:47-58, November 2018.

Paper 4. Guglielmo Minelli, Erwin Adi Hartono, Valery Chernoray, Linus Hjelm, and Siniša Krajnović. *Aerodynamic Flow Control for a Generic Truck Cabin Using Synthetic Jets*. Journal of Wind Engineering and Industrial Aerodynamics 168:81-90. September 2017. DOI: 10.1016/j.jweia.2017.05.006

Paper 5 Guglielmo Minelli, Erwin Adi Hartono, Valery Chernoray, Linus Hjelm, Branislav Basara, and Siniša Krajnović. *Validation of PANS and Active Flow Control for a Generic Truck Cabin*. Journal of Wind Engineering and Industrial Aerodynamics 171:148-160. December 2017.

Other publications:

Paper 6. Guglielmo Minelli, Erwin Adi Hartono, Valery Chernoray, Linus Hjelm, Branislav Basara, and Siniša Krajnović. *Development of Active Flow control for Trucks*. 3rd Thermal and Fluids Engineering Conference. January 2018. DOI: 10.1615/TFEC2018.tff.021216

Paper 7. Guglielmo Minelli, Erwin Adi Hartono, Valery Chernoray Linus Hjelm, Siniša Krajnović, and Branislav Basara. *PANS Validation and Active Flow Control for a Simplified Truck Cabin*. 16th European Turbulence Conference, 21-24 August, 2017, Stockholm, Sweden

-
- Paper 8.** Guglielmo Minelli, **Erwin Adi Hartono**, Sinisa Krajnovic, Valery Chernoray, and Linus Hjelm. *Flow Control for a Generic Truck Cabin Using Synthetic Jet*. European Drag Reduction and Flow Control Meeting – EDR-FCM 2017 April 3–6, 2017, Rome, Italy
- Paper 9.** Guglielmo Minelli, **Erwin Adi Hartono**, Linus Hjelm, Valery Chernoray, Branislav Basara, Siniša Krajnović. *Experimental And Numerical Investigation Of Active Flow Control On a Generic Truck Cabin*. 11th International ERCOFTAC Symposium on Engineering Turbulence Modelling and Measurement, Palermo, Italy. September 2016.
- Paper 10.** Xin Zhao, Mikhail Tokarev, **Erwin Adi Hartono**, Valery Chernoray, Tomas Grönstedt. *Experimental Validation Of the Aerodynamic Performance Of an Aero Engine Intercooler*. Journal of Engineering for Gas Turbines and Power 139(5). 2016. DOI: 10.1115/1.4034964
- Paper 11.** **Erwin Adi Hartono**, Maxim Golubev, Pirooz Moradnia, Valery Chernoray, Håkan Nilsson. *PIV Measurement of Air Flow in a Hydro Power Generator Model*. Proceedings of 16th International Symposium on Applications of Laser Techniques to Fluid Mechanics. Lisbon, Portugal, 09-12 July, 2012.

List of Acronyms

2C-2D	–	Two components two dimensional
3C-2D	–	Three components two dimensional
AFC	–	Active Flow Control
CFC	–	Chlorofluorocarbons
CFD	–	Computational Fluid Dynamics
CCA	–	Constant Current Anemometry
CTA	–	Constant Temperature Anemometry
CVA	–	Constant Voltage Anemometry
CO ₂	–	Carbon Dioxide
FZG	–	Forschungsstelle für Zahnrad und Getriebebau (Research Center for Gear Wheels and Gear Construction)
LES	–	Large Eddy Simulation
PANS	–	Partially Averaged Navier Stokes
PIV	–	Particle Image Velocimetry
PMMA	–	Poly(methyl methacrylate) also known as acrylic or acrylic glass
SPH	–	Smoothed Particle Hydrodynamics

Contents

Abstract	v
Acknowledgments	vii
List of Publications	ix
List of Acronyms	xi
I Introductory chapters	1
1 Introduction	3
1.1 Power losses inside the transmission	4
1.1.1 Churning losses	4
1.1.2 Challenges of the churning losses problem	5
1.1.3 Previous studies on the churning losses problem	5
1.1.4 Scope of the churning losses study	5
1.2 Aerodynamic resistance in truck	6
1.2.1 Challenges for aerodynamic drag problem in trucks	6
1.2.2 Active Flow Control (AFC)	7
1.2.3 Scope of the AFC study	8
2 Experimental Apparatus	9
2.1 Churning losses study	9
2.1.1 Chalmers gear test rig	9
2.1.2 Flash photography & High speed recording	11
2.1.3 Torque measurement	11
2.2 Active flow control study	13
2.2.1 Chalmers wind tunnel	13
2.2.2 Generic truck cabin	13
2.2.3 Hot wire anemometry	14
2.2.4 Static pressure measurement	14

3	Particle Image Velocimetry (PIV)	17
3.1	PIV basic principles	17
3.2	PIV setup	18
3.2.1	Planar PIV	18
3.2.2	Stereo-PIV	18
3.2.3	Time-resolved / high speed PIV	19
3.3	Additional equipment to support PIV measurement	20
3.3.1	Liquid prism	20
3.3.2	Fluorescent tracers	20
3.3.3	Refraction index matching	21
4	Summary of Appended Papers	23
4.1	Paper 1	23
4.2	Paper 2	25
4.3	Paper 3	27
4.4	Paper 4	31
4.5	Paper 5	32
5	Unpublished Results on Churning Losses Study	35
5.1	Aeration	35
5.2	Comparison between gear and cylinder with the same outer dimensions	40
5.3	Curve fit of torque data using machine learning	43
6	Concluding Remarks	47
6.1	Conclusion	47
6.1.1	Churning losses inside a transmission	47
6.1.2	Active flow control	47
6.2	Recommendation for future works	48
6.2.1	Churning losses inside a transmission	48
6.2.2	Active flow control	49
II	Appended papers	55
1	PIV Study of Fluid Flow Inside A Gearbox	57
2	Stereo-PIV Study of Oil Flow Inside a Model Gearbox	71
3	Numerical simulations of oil flow inside a gearbox by Smoothed Particle Hydrodynamics (SPH) method	81
4	Aerodynamic Flow Control for a Generic Truck Cabin Using Synthetic Jets	95
5	Validation of PANS and Active Flow Control for a Generic Truck Cabin	107

Part I

Introductory chapters

Chapter 1

Introduction

Global warming is a real threat to the existence of humankind. It leads to more extreme weather conditions, the acidification of the sea, increasing sea levels due to the melting of the ice caps, and the warming of the ocean. CO₂ gases combined with other greenhouse gases (water vapour, methane, nitrous oxide, and CFCs) are believed to cause global warming. Human activities play a large part in disturbing the balance of the natural absorption and discharge of CO₂ gases to the atmosphere. It is estimated that more than a third of CO₂ concentration since the industrial revolution in the eighteenth century has been caused by human activity [1]. The transport sector (including aviation but excluding international shipping) contributes to around 26% of total EU-28 greenhouse gas emissions. Road transport (cars, buses, light and heavy duty trucks, motorcycles, and other road transportation) makes up almost 73% of these emissions [2].

Attempts have been made by policy makers to reduce CO₂ emissions: ever stricter regulations regarding CO₂ emissions of road transport have been created and implemented (e.g. Euro 1-6). These demanding legislation changes force vehicle manufacturers to innovate and continuously improve their products. For heavy duty vehicles there are five areas that are considered when calculating the total CO₂ contribution. These are engine, transmission, rear axle, rolling resistance (tyres), and aerodynamic resistance [3]. Figure 1.1 shows a breakdown of the energy usage of trucks and buses. In the figure, the individual contributions of the components seem small. However, a significant reduction of the total CO₂ emission can be achieved if each of the components is improved simultaneously.

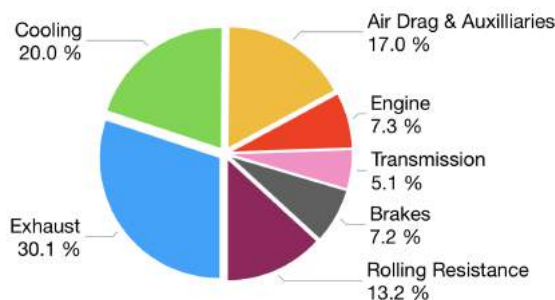


Figure 1.1: Breakdown of the energy usage of trucks and buses [3]

In this study transmission power losses in terms of churning losses and active flow control to reduce the aerodynamic resistance in terms of separation in the A-pillar are studied. Both studies shed light on the two topics: churning losses and active flow control. This work compliments existing knowledge on the above topics and is proven to be useful by providing additional data for validations of numerical simulations.

1.1 Power losses inside the transmission

If we take a closer look at transmissions, power losses inside a transmission are composed of two groups: load dependent power losses and load independent power losses [4]. Load dependent power losses stem from solid friction. The friction varies with the load and occurs when two surfaces in mechanical contact move relative to each other. Load independent power losses stem from fluid friction. Fluid friction varies with rotational speed and temperature. Load independent power losses are also called no-load losses or spin power losses. Losses such as churning losses, windage losses, and squeezing/pocketing losses are examples of no-load losses. An illustration of churning, windage, and squeezing/pocketing losses can be found in Figure 1.2.

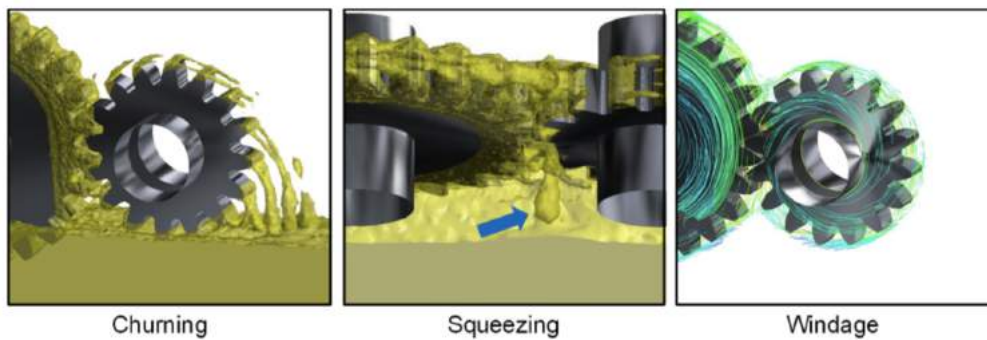


Figure 1.2: Illustration of types of load independent power losses from [5]

1.1.1 Churning losses

The standard lubrication system for heavy duty vehicles is a combination of dip/splash and force feed/circulating lubrication. Complete presentation of the lubrication systems and guidelines on how to select a lubrication system can be found in [6]. In the dip/splash lubrication system, the gears are partially immersed in an oil bath. As the gears rotate, they generate splash, which can provide some lubrication to the pinion, bearings, seals, and other auxiliaries. The force feed is added to assist lubrication for bearings, and other components inside the transmission which are far from splash. The immersion of the gear teeth is important to dissipate the heat, wash out contaminants, and coat the gear surface for protection against corrosion, as well as providing a thin film to prevent metal-to-metal contact (reducing friction) [7]. One of the drawbacks of a dip lubrication system is that the rotation also churns the oil, which in turn generates losses called churning losses.

1.1.2 Challenges of the churning losses problem

It is obvious that reducing the immersion depth of the gears minimises the churning losses. However, the durability/lifetime of the gears is also greatly reduced when the immersion depth is at its minimum due to lack of heat dissipation [8]. Using low viscosity oil reduces churning losses; however it is prone to high temperatures, where it can lose its ability to provide sufficient film thickness to prevent metal to metal contact. Removing the oil bath completely and changing to a spray lubrication system can also reduce churning losses; however, additional devices in the system mean extra energy and added complexity that needs to be addressed. Certainly, reducing churning losses is not a straightforward task. It is a challenge to find a balance between sufficient lubrication, good heat dissipation, and low power losses. It requires a good understanding of fluid dynamics and heat transfer, especially when durability, reliability, and efficiency are paramount requirements.

1.1.3 Previous studies on the churning losses problem

The advance of computers makes numerical simulations more feasible than before. This means that in certain situations, a numerical simulation is a realistic method to choose. Oil flow inside a transmission is a complex flow phenomenon due to multiphase and turbulent flow. In addition to this, transmission is usually made as compact as possible, due to space constraints in the vehicle. These factors make the study of oil flow experimentally challenging and the number of such studies already in existence is limited. Numerical simulations do not share this problem. This is perhaps why recent publications on this topic tend to utilise numerical simulations (e.g. [9], [10], [11], [12], and [13]). These studies showed great potential to be a development tool for optimising the oil flow inside a transmission. However, the experimental studies which support the simulations usually come in the form of qualitative studies, such as comparisons with flow visualisation images (e.g. [14], and [15]). For numerical models to be reliable, good quantitative data is needed to develop the model (e.g. [16]). Other experimental studies on this topic usually aim to study the durability of the gear teeth (e.g. [17]) or to find the torque loss correlation (e.g. [18], [19], and [20]).

1.1.4 Scope of the churning losses study

The present study investigates churning losses of a pair of spur gears partially immersed in a rectangular gearbox from a fluid dynamics point of view. Details about the test object and the experimental apparatus are discussed in chapter 2. The churning oil flow is investigated by means of flow visualisation, velocity and torque measurement. Additional findings related to aeration, comparison between a spur gear and a cylinder, and a curve fitting technique using machine learning to find the exponent of the churning loss equation are discussed in chapter 5. A conclusion and recommendations for future work are presented in chapter 6.

1.2 Aerodynamic resistance in truck

Aerodynamic resistance (air drag) is one of the largest resistances in trucks after the rolling resistance (see Figure 1.1). The air drag is especially important for long haul trucks, which spent most of their lifetimes cruising at highway speed. Air drag increases exponentially as it is a function of velocity squared, as explained in this formula $D = 0.5C_d\rho v^2 A$, where D is the air drag, C_d is the coefficient of drag, ρ is the density of air, v is the air velocity and A is the frontal area of the vehicle. Figure 1.3 shows a schematic comparison between the aerodynamics drag and rolling resistance in terms of velocity.

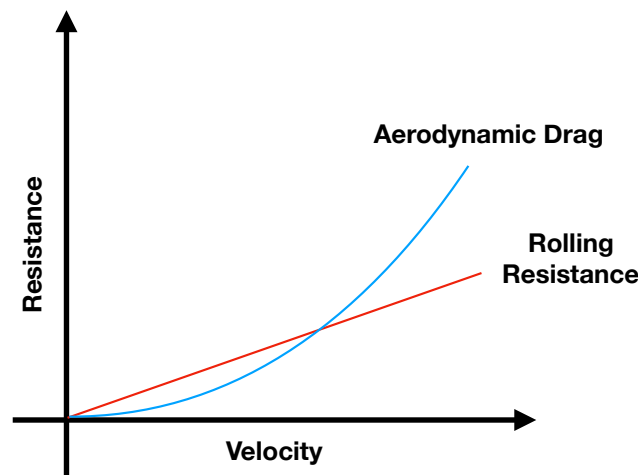


Figure 1.3: Schematic of the development of aerodynamics and rolling resistance with velocity

Aerodynamic resistance in a truck stems from flow separation. For truck applications, flow separation happens in several locations, such as in the A-pillar, mirrors, wheel and under-body, wake of the trailer, in the frontal area of the trailer, and the gap between tractor and trailer. Figure 1.4 illustrates these flow separation locations on a truck.

1.2.1 Challenges for aerodynamic drag problem in trucks

In fluid dynamics studies, the body of the truck is considered to be a bluff body. Bluff body aerodynamics are characterised by a large separation and low pressure wake behind the object. The pressure difference between the front (the stagnation point) and rear (the wake) of the bluff body defines the magnitude of the pressure drag. This means that reducing the pressure drag can be achieved by reducing/altering the wake size and/or increasing the pressure recovery [21]. An easy way to achieve this is by streamlining. Unfortunately it is not that easy in truck applications to modify the shape of tractors/trailers due to strict dimension requirements in terms of maximum cargo capacity. Therefore, further studies in the field of fluid dynamics are needed

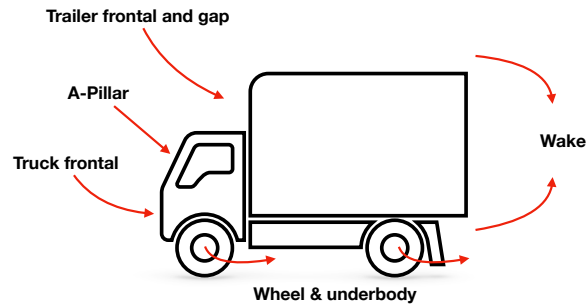


Figure 1.4: Schematic of the locations of the separate regions of the truck

to better understand the mechanisms of flow separation and how to possibly control flow separation.

1.2.2 Active Flow Control (AFC)

In general, the flow control for bluff body separation can be divided into two categories: active and passive. The passive way to control flow separation is the first to make an appearance in the real application because of its simplicity and lower implementation cost. An example of passive flow control for trucks can be found in [22]. Figure 1.5 shows an illustration of some of the passive flow controls that can be found in trucks. However, the actual wind direction is not always parallel to the direction of the truck. Therefore, passive flow control does not always work as intended.

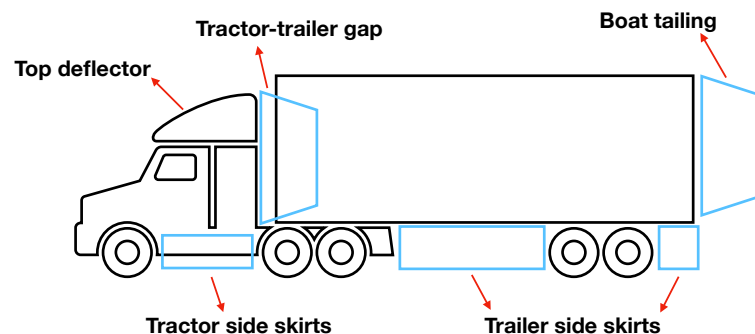


Figure 1.5: Schematic of passive flow control in a truck

An AFC works differently from the passive counterparts. It targets the fluid inside the boundary layer and manipulates the fluid kinetic energy to prevent/promote

separation. The AFC also changes the mixing properties of the separated shear layer to prevent/promote reattachment [23]. The active flow control opens the possibility of performing feedback control of the boundary layer and thereby control flow separation.

If we look at the topology of the fluid flow separated from the rounded corner of the A-pillar, it is to some extent analogous with the stalled airfoil. The separated flow is characterised by shear layer and wake shedding. Previous studies in the aeronautic field show that an active flow control using a synthetic jet was able to suppress the separation in the airfoil [24]. Inspired by work on the aeronautic field, a flow control for the A-pillar separation in the truck is studied.

1.2.3 Scope of the AFC study

The present study looks into the flow velocity field and pressure distribution around the generic truck cabin with and without AFC. The model was built to represent the flow separation at the A-pillar of the truck cabin. Details of the test object and the experimental apparatus are discussed in chapter 2. The flow velocity is investigated by means of time-resolved particle image velocimetry. The pressure distribution is investigated by means of static pressure measurement. The synthetic jet is characterised by means of hot wire anemometry. The conclusion and future work are presented in chapter 6.

Chapter 2

Experimental Apparatus

2.1 Churning losses study

2.1.1 Chalmers gear test rig

A new special test rig was required to perform this study. The reason is that the real transmission is highly complex and its geometry can often be considered confidential information. Therefore, it was necessary to have a simple and generic transmission that could be easily modified to accommodate the needs of PIV measurement. An FZG gear test rig [25] was chosen to be the baseline of the Chalmers gear test rig. Some modifications were made to the original design of the FZG gear test rig to fit the needs of the present study. The modifications focused on optical access and simplifying the test rig. The test section and the gears were made from PMMA in order to maximise optical access. The loading arm was removed in this study because loading the gear teeth does not change the oil flow inside. The drive gears were replaced with a belt drive to reduce the total weight of the test rig. A heater was added to regulate the oil temperature, due to no torque transfer and high dissipation rate through the aluminium wall. Figure 2.1 shows a side by side schematic comparison of the Chalmers gear test rig and the FZG gear test rig.

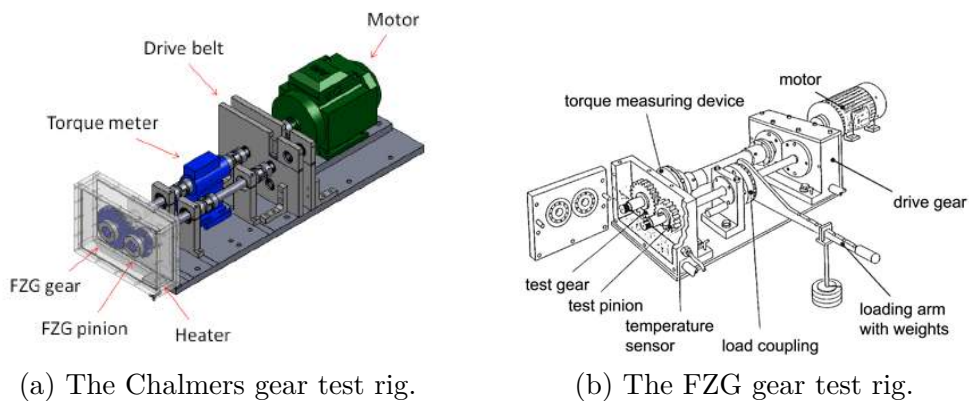
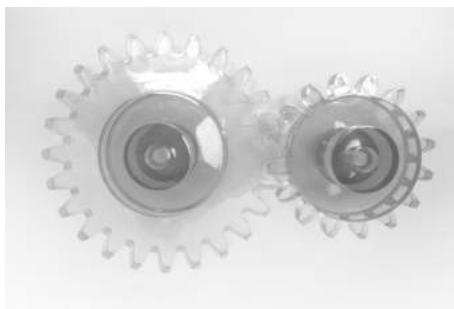


Figure 2.1: The test rig side by side comparison

Test objects

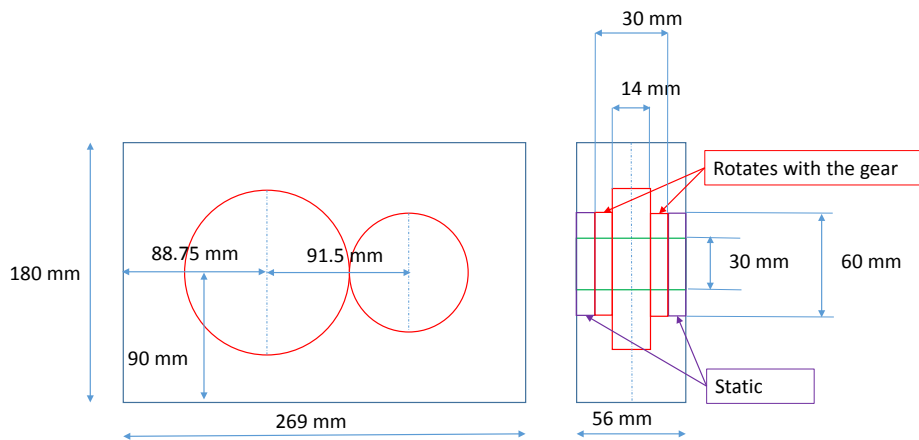
The test objects consisted of a pair of spur gears and a pair of cylinders. The spur gear pair geometry was based on the FZG gear type C [25]. The cylinder pair was based on the dimensions of the spur gears. They were used to study the possibility of simplifying the gear geometry in numerical simulations. Figure 2.2 shows the gear, the pinion, the cylinders and detailed dimensions of the test section. Table 2.1 shows the specifications of the gear, the pinion, and the cylinders.



(a) The gear and pinion



(b) The cylinder gear and pinion



(c) The detailed dimensions of the test section

Figure 2.2: The test objects for the churning losses study

Test oil

The oil used in this study was Nytex 810 from Nynas, which has a clear appearance, again chosen to maximise optical access. The viscosity of the oil was held approximately constant throughout the study by maintaining the oil temperature at around 20-30°C. Table 2.2 partially shows the specifications of the test oil. The full

Parameter	Unit	FZG Gear	FZG Pinion	Cylinder Gear	Cylinder Pinion
Number of teeth	-	24	16	-	-
Module	mm	4.5	4.5	-	-
Centre distance	mm	91.5	91.5	91.5	91.5
Face width	mm	14	14	14	14
Tip diameter	mm	118.4	82.5	120	60
Pitch diameter	mm	109.8	73.2	-	-

Table 2.1: Dimensions of the gears and the cylinders

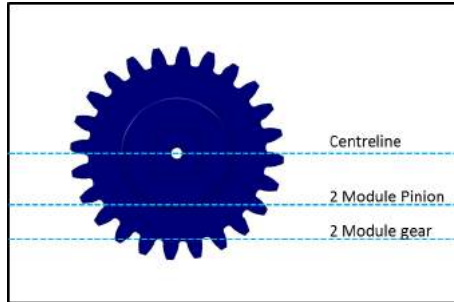


Figure 2.3: Oil level (schematic)

Property	Unit	Data
Density, 15°C	kg/cm^3	901
Viscosity, @ 40°C	cSt	22.4
Viscosity, @ 100°C	cSt	3.7
Refractive index, 20°C	-	1.493
Appearance	-	clear

Table 2.2: The oil properties

specifications of the oil can be found in [26]. Figure 2.3 illustrates the three different oil levels used in the PIV study.

2.1.2 Flash photography & High speed recording

Fluid mechanics have had a long relationship with flow visualisation. Flow visualisation is used as a fast exploratory tool which aims at the discovery, description, and investigation of global flow field information [27]. In this study, the quasi-steady state of the oil flow inside a gearbox was investigated using flash photography.

Figure 2.4 shows a schematic of the flash photography setup. A DSLR camera (Nikon D3200) equipped with a 35 mm lens (Nikon) was set in front of the test section. The camera was located at a distance at which each corner of the test section frontal face was visible from the viewfinder. An external flash unit (Nikon SB-700) was located directly above the test section, pointing downward at a distance of 40 cm. The flash power was 1/8 of the max power. The flash duration for the Nikon SB-700 can be found in [28]. Two reflectors (not shown in the figure) were located on both sides of the test section to redistribute the light and minimise the shadows.

The high speed recording was done using Nikon V1 with 400 fps frame rate. The camera setup is the same as the flash photography setup (see Figure 2.4). The camera was located in front of the test section. The illumination was done using an ordinary fluorescent lamp.

2.1.3 Torque measurement

Torque measurement gives a direct indication of the load independent power losses. The torque meter directly measured how much torque is needed to rotate the gear.

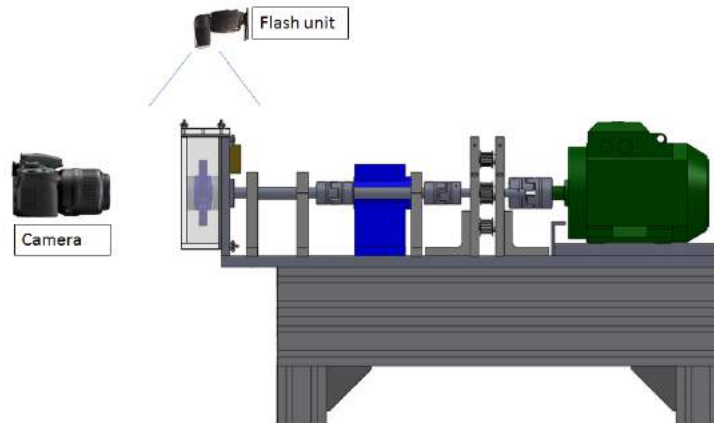


Figure 2.4: The schematic of the flash photography setup.

The torque loss contribution from the presence of oil can be calculated by subtracting the torque value of the measurement with the oil from the torque measurement without the oil.

In this study, the torque was measured using a KISTLER torque sensor (variant number: 4503A20L00B1CD1). Figure 2.5a shows a schematic of the torque meter in the test rig. The sensor was situated in between the motor and the test section, which measured the torque transferred to the gear or to the pinion depending on the axis on which it was mounted. Figure 2.5b shows an illustration of the immersion depths used during the torque measurement. Three different immersion depths were used.

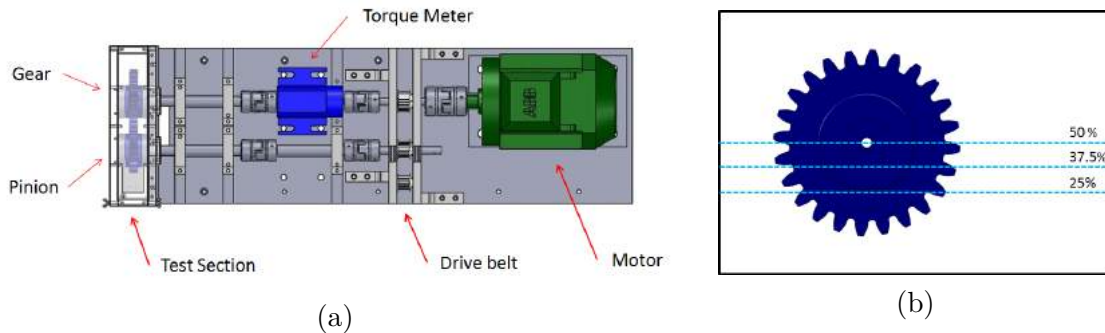


Figure 2.5: (a) Schematic of the torque meter placement and (b) the immersion depth for the torque study. Note that the oil level definition for torque measurement is slightly different from the PIV measurement in Figure 2.3.

The torque loss was measured for seven speed steps (250, 500, 750, 1000, 1500, 2000, 3000 RPM). The torque was measured both ways, from low to high speed and from high to low speed. These measurements were repeated three times. At every speed step five readings were taken with a two second interval between each reading. Every measured torque was measured for an average of two seconds. This gave a total of thirty torque readings per speed step. The collected data was then analysed by using median absolute deviation to remove outliers. Afterwards, the collected

data was averaged. The averaged collected torque data was the churning loss at a particular speed after subtraction of the mechanical losses in the system.

2.2 Active flow control study

2.2.1 Chalmers wind tunnel

The Chalmers wind tunnel is a closed circuit wind tunnel at Fluid Dynamics Division, Mechanics and Maritime Sciences Department, Chalmers University of Technology, Sweden. Figure 2.6 shows a schematic of the Chalmers wind tunnel. The wind tunnel's test section is 3 metres in length, 1.8 metres in width and 1.25 metres in height. The velocity range is from 0 up to 60 m/s .

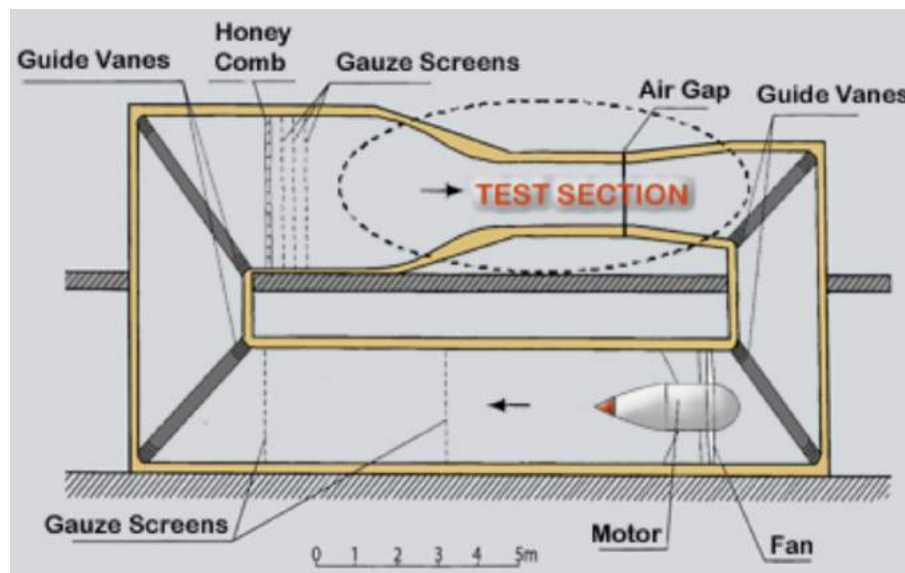


Figure 2.6: Schematic of the Chalmers wind tunnel

2.2.2 Generic truck cabin

The test object for the AFC study is a hollow cube with rounded corners which has a 1 mm slit at a 45° angle. It was built to simulate a simplified version of the truck cabin. Figure 2.7 shows the test object. It has external dimensions of $W = 0.4$ m and $L = 0.36$ m. There were four loudspeakers inside the cube, each with a diameter D of 0.18 m, serving as flow control actuators. When the speakers were supplied with a sinusoidal signal, their membranes moved back and forth, creating blowing and suction through the slit. The cube was located in the middle of the wind tunnel test section, which has height, $K = 1.25$ m and width, $S = 1.80$ m. The cube was supported by a cylindrical holder that was covered by an NACA profile to reduce the flow disturbances coming from the holder.

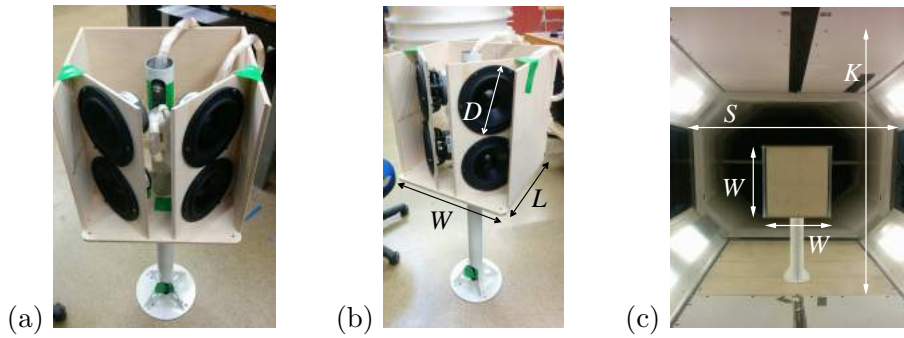


Figure 2.7: The generic truck cabin [29]

2.2.3 Hot wire anemometry

Hot wire anemometry is a flow velocity and temperature measurement technique which utilises heat transfer from a heated sensor exposed to the fluid in motion. There are three common regimes for hot wire operation: CTA, CCA, and CVA. Details about the hot wire anemometry are beyond the scope of this thesis and the interested reader should consult [30].

In this study, a single wire configuration with constant temperature anemometry method was used to estimate the magnitude of flow velocity out of the slot that was produced by the speaker. Different amplitudes and frequencies of the sinusoidal wave were tested to characterise the speaker. The chosen frequency and amplitude were 50 Hz at 1.4 V, 100 Hz at 1.4 V, 150 Hz at 2.5 V, and 300 Hz at 6 V. The measurements were done in the middle of the slit with a fixed distance of 4.25 mm, as shown in Figure 2.8.



Figure 2.8: The hot wire anemometry setup

2.2.4 Static pressure measurement

Static pressure measurements on the surfaces of the test object were done with a series of pressure taps at the mid-plane along the front, side, and rear of the test object. Figure 2.8 shows the pressure taps at the front and side faces. Time-averaged

two second measurements were done in order to evaluate the coefficient of pressure, C_p . Two yaw angle configurations, 0° and 10° were measured.

Chapter 3

Particle Image Velocimetry (PIV)

Fluid flow can be disturbed by the presence of a measurement device. This is especially true for oil flow measurement inside a gearbox, which has a relatively tight space inside. The solution is to choose a non-intrusive measurement technique. One of the most non-intrusive, indirect and optical fluid velocity measurements is PIV. Details about PIV in general are beyond the scope of this thesis and can be found [31] or [32].

3.1 PIV basic principles

Figure 3.1 shows a schematic of the PIV in the wind tunnel. Particles (seeding) were added to the fluid in order to visualise the flow. Two consecutive images with known time intervals were recorded. A laser was used as a means of light source due to its ability to produce high intensity light with short duration. The displacement of the particles was evaluated by means of statistical method (cross-correlation). The flow velocity vector was evaluated from the displacement and the time interval.

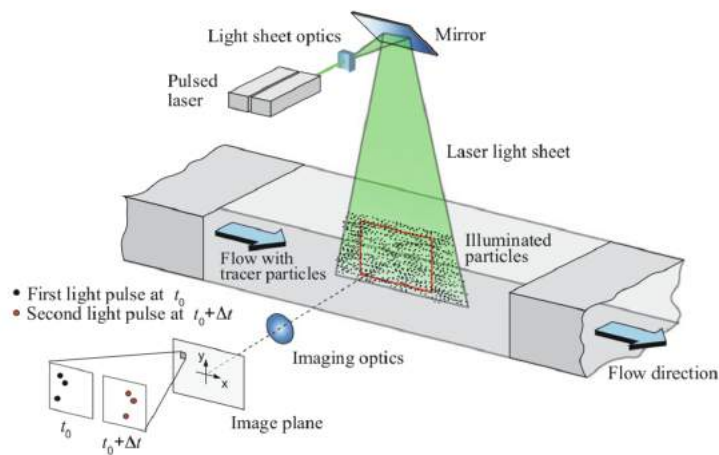


Figure 3.1: The schematic of the planar PIV setup in the wind tunnel [32]

3.2 PIV setup

There are many types of PIV setup. The most frequently used are as follows: planar (2C-2D) PIV, stereoscopic (3C-2D) PIV, tomographic (volumetric, 3C-3D) PIV, micro PIV, time-resolved/high speed PIV. The illumination sources are characterised by repetition rate and illumination thickness. The cameras are characterised by sensor speed, lens magnification, and resolution. A PIV setup which combines a slow speed sensor camera with a slow repetition rate laser with thin sheet illumination is called a planar PIV. If we add one more camera to the planar PIV setup and set the angle between the cameras in a way that fulfills Scheimpflug criteria, the PIV setup is now called stereoscopic PIV. If we replace the camera and the laser with a high speed sensor and a high repetition rate laser, the PIV setup is called time resolved.¹

In this study, planar PIV, stereo-PIV and time-resolved PIV were used. Details of the setup can be found in [29], [33], and [34].

3.2.1 Planar PIV

Planar PIV is sometimes called 2C-2D PIV. The name stems from its ability to measure two components of velocity vectors in two-dimensional spaces (a plane). It is the simplest PIV setup. It involves pointing one camera so that its vision is perpendicular to the laser sheet. Figure 3.2 shows the setup of the planar PIV that is used to measure the midplane velocity field of the oil flow inside the transmission. Details about setup and results can be found in [33]. One main drawback of the planar PIV is that if the flow in the measurement plane is highly three-dimensional, the tracer particles can move out of the measurement plane, causing an error in the measurement. One way of solving this issue is to add additional viewing directions.

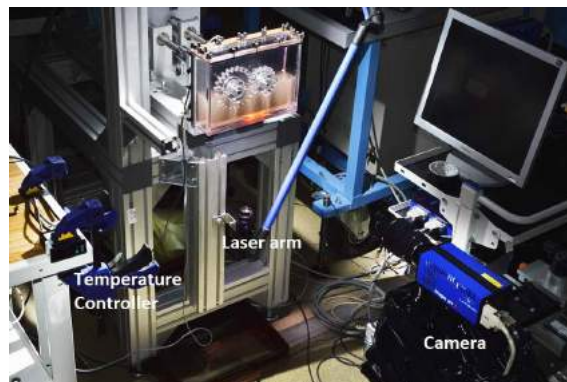


Figure 3.2: 2C-2D PIV setup for the churning losses study

3.2.2 Stereo-PIV

Stereo-PIV is a PIV measurement technique which utilises a second viewing direction. The second viewing direction is usually achieved by using a second camera. The

¹The naming time resolved is valid if the temporal resolution of the flow field is really resolved otherwise it should be called high speed [32]

additional camera enables full reconstruction of velocity components and leads to better accuracy for three-dimensional flow. Figure 3.3 shows the stereo-PIV setup used in this study to measure the oil flow inside the transmission.

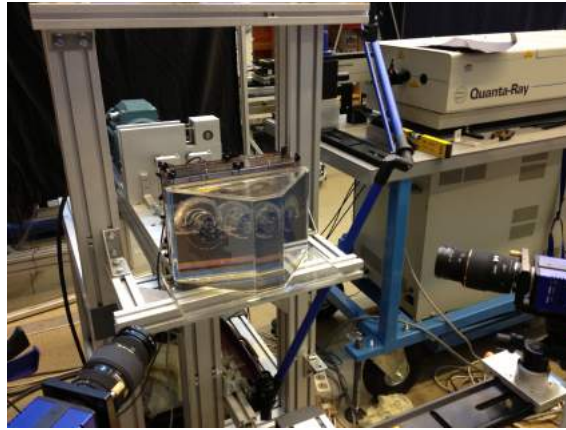


Figure 3.3: 3C-2D Stereo-PIV setup for the churning losses study

3.2.3 Time-resolved / high speed PIV

The invention of high speed CMOS sensors and high speed lasers enabled PIV measurements to resolve temporally well flow field of low-speed aerodynamic flows. In this study, high speed PIV measurement was done to study the flow separation in the A-pillar of a truck cabin with and without active flow control. Figure 3.4 shows the experimental setup of the high speed PIV used in this study.

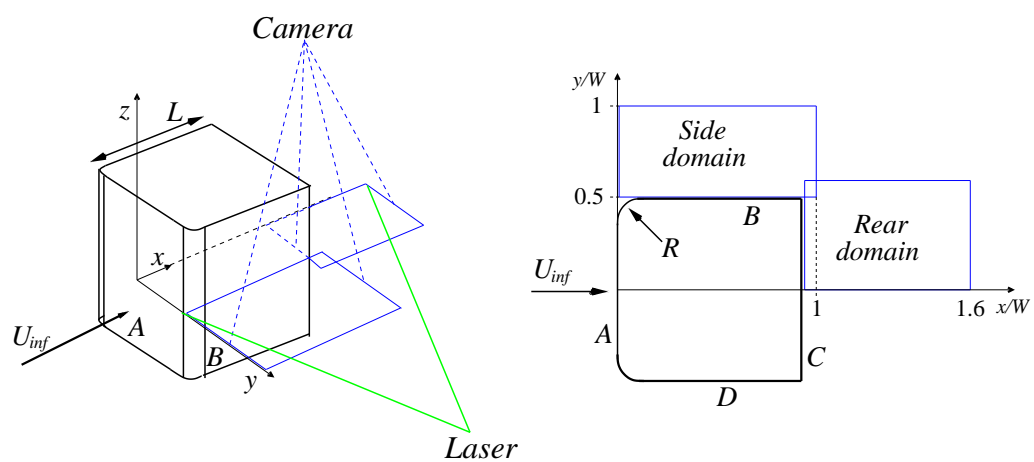


Figure 3.4: 2C-2D Time-resolved PIV setup for the AFC study

3.3 Additional equipment to support PIV measurement

3.3.1 Liquid prism

Stereo PIV measurement requires two cameras to be located at an oblique angle from the axial axis, in order to fulfill the Scheimpflug criterion. At air-liquid interface this condition poses a problem, i.e. optical aberration. In order to solve the issue and maintain an orthogonal view with respect to the liquid-air-interface, a liquid prism was built and attached to the front of the test section. Figure 3.5 shows the stereo PIV schematic setup with the liquid prism attached.

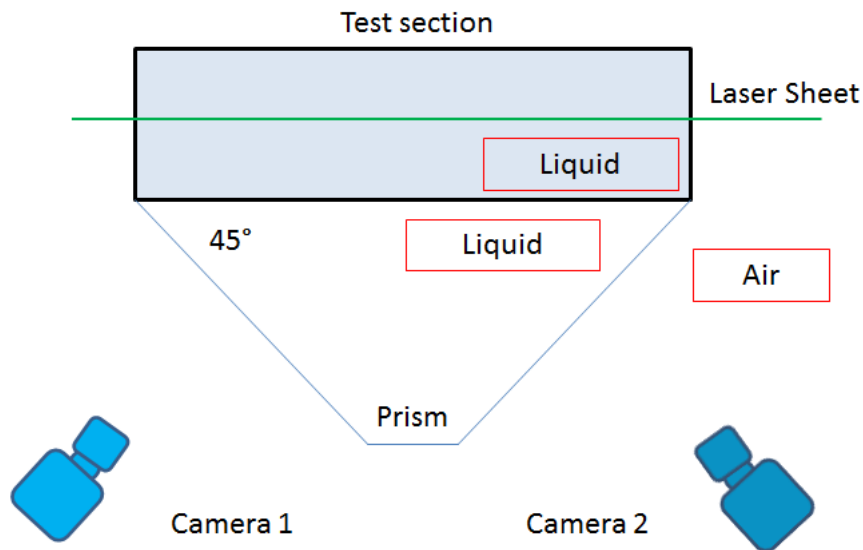


Figure 3.5: The schematic of stereo-PIV setup with liquid prism attached

3.3.2 Fluorescent tracers

In the study of oil flow inside a transmission, a large number of bubbles are generated when the gears rotate. The mechanism behind the bubble generation inside the transmission will be discussed in section 5.1. These bubbles come in various sizes and, although they can act as tracer particles, they are not a suitable choice for PIV measurement. This is because only the bubble edges and the very small bubbles that follow the flow faithfully generate strong reflection of the laser illumination. In order to tackle this problem, melamine-based particles with rhodamine B colouring agent (fluorescent particles [35]) are used in this study. The fluorescent dye absorbs the incident light and emits it at a longer wavelength. In combination with an optical filter that allowed only a certain wavelength, the reflection from the bubbles were suppressed. Figure 3.6 shows a comparison of the PIV raw images using only bubbles and fluorescent particles. Note that the bright spots due to reflection were reduced significantly.

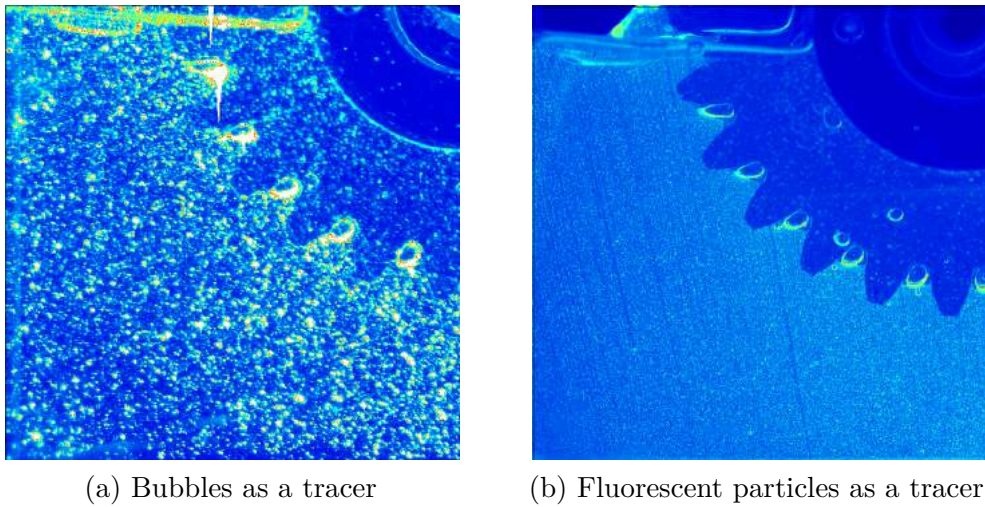


Figure 3.6: Comparison of the raw images from PIV camera

3.3.3 Refraction index matching

Good optical access is paramount for PIV measurement. Another way to enhance optical access is to use refractive index matching. By selecting a refractive index that is between the test object (1.491) and the test oil (1.494), the outline of the test object appears to be invisible inside the test oil. Figure 3.7 shows the result of refractive index matching.

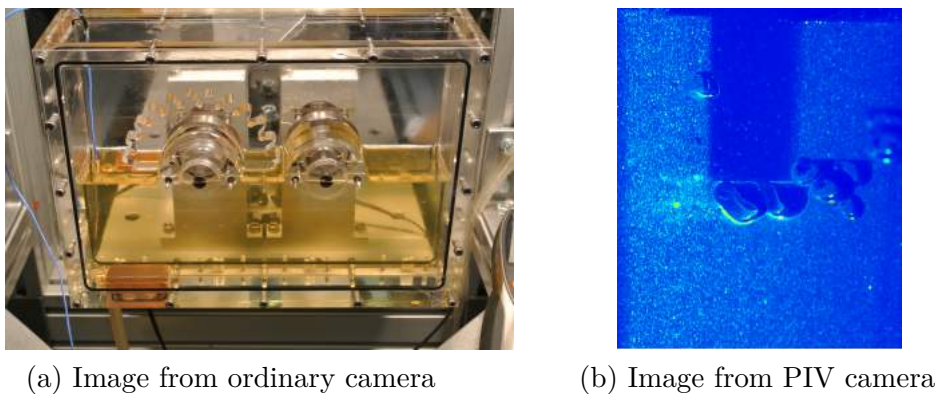


Figure 3.7: Refractive index matching between the test object and test oil

Chapter 4

Summary of Appended Papers

4.1 Paper 1

Erwin Adi Hartono, Maxim Golubev, and Valery Chernoray. *PIV Study of Fluid Flow Inside a Gearbox*. Proceedings of the 10th International Symposium on Particle Image Velocimetry - PIV13. Delft, The Netherlands. 1-3 July, 2013.

Division of work

Erwin Adi Hartono designed the test rig, set the test cases, performed the flow visualisation study, performed the PIV measurement, post processed the experimental data, wrote the paper, and presented the paper at the conference. Maxim Golubev helped with the PIV measurement, and gave feedback on the paper. Valery Chernoray gave feedback and supervised the work.

Summary

In this paper, flow visualisation and PIV measurement of oil flow around a pair of spur gears inside a gearbox were done. Quasi-steady state flow for three different oil levels (centreline, 2 module pinion, and 2 module gear) and nine different rotational speeds were captured by flash photography. The results suggest that the oil flow is governed by the larger diameter gear. Deeper immersion results in more stirring and dragging of oil from the oil sump, creating higher and larger splash. The splash distribution was observed to be more towards the gear side than the pinion side. Oil level drop was observed and more prominent (up to 20 mm) at high rotational speed. The bubble generation (aeration) level was observed to be higher for the high rotational speed when a quasi-steady state was reached. This was the limiting factor for the PIV measurement. Figure 4.1 shows a side by side comparison between low ($V_t = 0.55m/s$) and high ($V_t = 2.64m/s$) rotational speeds for the centreline immersion depth case.

PIV measurements were done with three different oil levels (same as the flow visualisation), three different rotational speeds (0.55, 1.1, and 1.62 m/s) and three

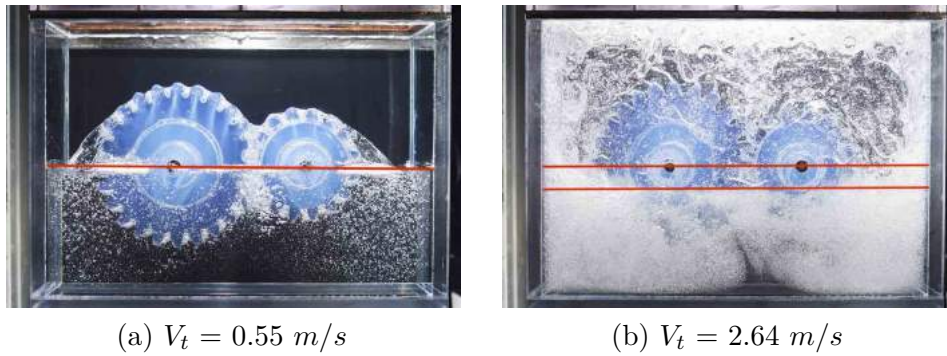


Figure 4.1: Immersion depth drop comparison and aeration level of two rotational speeds.

different locations in the mid-plane of the test section. The rotational speed was limited due to high aeration levels. PIV measurement in the mid-plane revealed that oil was recirculated below the gear and the pinion wheel. The area between the gear and the pinion would be the region where the two flows meet; this is where the stagnation region is located. Figure 4.2 shows a schematic of the three different measurement regions (a-c) and their corresponding velocity fields (d-f) for the centreline immersion depth and 0.55 m/s pitch line velocity. The overall view (a) is the full frontal view. The gear zoom view (b) is the quarter view below the gear. The pinion zoom view (c) is the quarter view below the pinion.

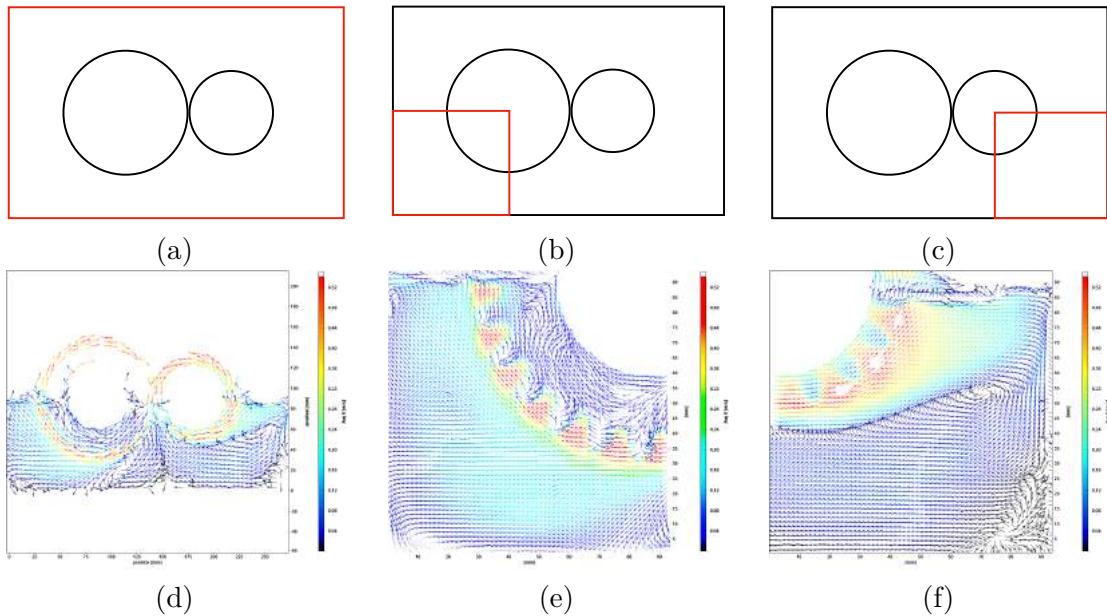


Figure 4.2: Schematic of the measurement regions (a-c) and the corresponding flow velocity fields (d-f). The overall view (a) is the full frontal view. The gear zoom view (b) is the quarter view below the gear. The pinion zoom view (c) is the quarter view below the pinion. The result is from the test case 0.55 m/s pitch line velocity and centreline immersion depth.

4.2 Paper 2

Erwin Adi Hartono, Alexandr Pavlenko, and Valery Chernoray. *Stereo-PIV Study of Oil Flow Inside a Model Gearbox*. Proceedings of the 17th International Symposium on Applications of Laser Techniques to Fluid Mechanics. Lisbon, Portugal. 07-10 July, 2014.

Division of work

Erwin Adi Hartono designed the test rig, set the test cases, performed the PIV measurement, post-processed the experimental data, wrote the paper, and presented the paper at the conference. Alexandr Pavlenko helped with the PIV measurement and gave feedback on the paper. Valery Chernoray gave feedback and supervised the work.

Summary

In this paper, stereo-PIV was used to quantify the three dimensional character of the oil flow around a pair of spur gears inside a gearbox. The test cases were 0.55 and 1.1 m/s pitch line velocity with centreline immersion depth. Quasi-steady state oil flow velocity at five measurement planes along the axial direction was measured. Cross flow below the gear wheel and in the gear meshing region was measured.

The three-dimensional velocity field below the gear wheel was reconstructed from the five measurement planes. Figure 4.3 shows the three-dimensional reconstruction of flow velocity from the five measurement planes.

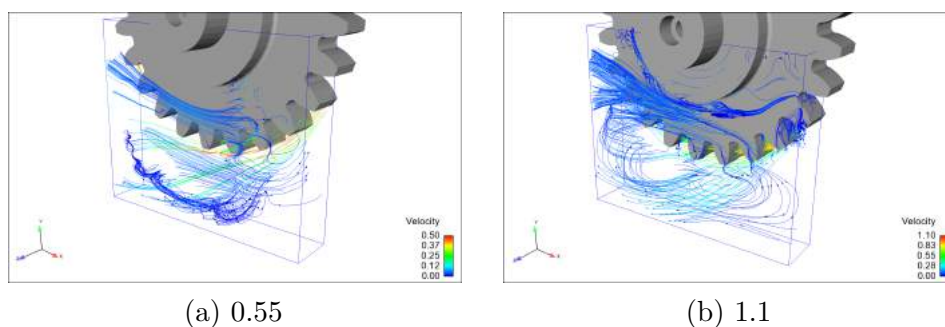


Figure 4.3: Three-dimensional reconstruction of oil velocity field from scanning PIV. Test case 0.55 and 1.1 m/s with centreline immersion depth.

The results for cross-flow measurement below the gear teeth reveal two vortices beside the gear teeth. The strength of the vortices is higher for the higher rotational speed case. This strengthens the hypothesis that the recirculation contributes to an increase in churning losses. Figure 4.4 shows the result of the cross-flow measurement under the gear wheel.

The result of cross-flow measurement at the meshing region shows the ejected oil from the meshing region (squeezing losses). Ejection was difficult to measure in this setup since the gear mesh region was close to the free surface region. The

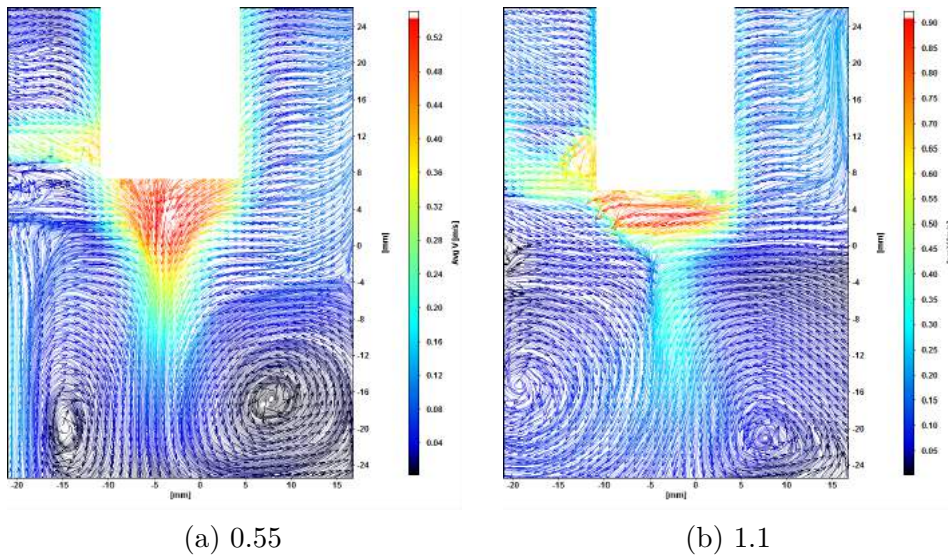


Figure 4.4: Cross-flow stereo-PIV under the gear wheel. Test case 0.55 and 1.1 m/s with centreline immersion depth.

results from the PIV measurement show flow velocity components in an axial direction, which can correspond to the ejection velocity. However, the magnitude is relatively small when compared to the recirculation. Figure 4.5 shows the result for the cross-flow PIV measurement at the meshing region.

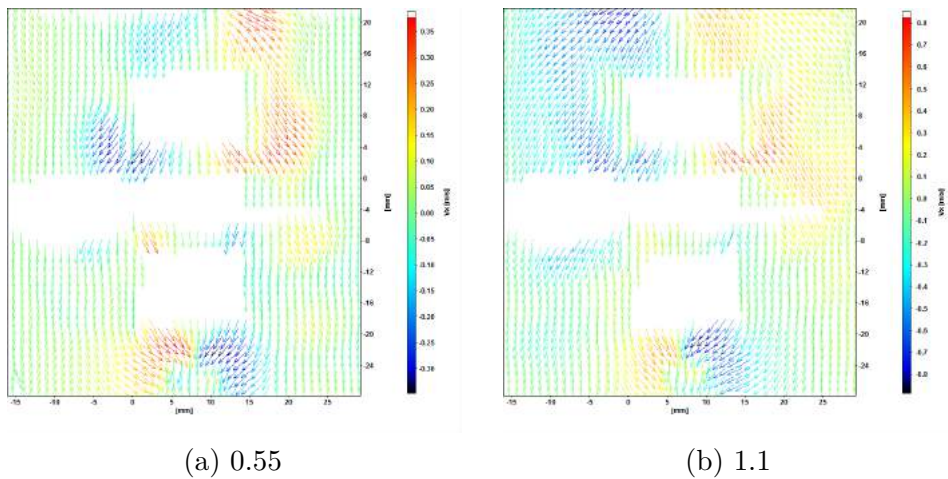


Figure 4.5: Cross-flow stereo-PIV velocity field in the gear meshing region. Test case 0.55 and 1.1 m/s with centreline immersion depth.

4.3 Paper 3

Zhe Ji, Miloš Stanić, Erwin Adi Hartono, and Valery Chernoray. *Numerical simulations of oil flow inside a gearbox by Smoothed Particle Hydrodynamics (SPH) method*. Tribology International, 127:47-58. November 2018.

Division of work

Zhe Ji performed the CFD simulation, wrote the paper, and submitted it to the journal. Miloš Stanić gave feedback and supervised the work. Erwin Adi Hartono performed the PIV measurement, post-processed the experimental data, performed discussion of CFD results, comparison of CFD and experiment, discussion of paper structure and entire paper content, feedback on CFD part and corrections of CFD part, and wrote the experimental part of the paper. Valery Chernoray gave feedback and supervised the work.

Summary

In this paper, numerical simulation (SPH) of a pair of spur gears inside a gearbox was compared and validated with experimental data. The test cases comprised three different rotational speeds ($v_t = 0.55, 1.1, 1.62 \text{ m/s}$) and three different immersion depths (centreline, 2-module pinion, and 2-module gear). Several aspects, such as aeration in terms of bubble size, velocity fields, and velocity profile below the gear teeth, were compared both qualitatively and quantitatively. The experimental data was gathered using 2C2D PIV. The data was phase averaged from 100 PIV images. Measurement uncertainty calculations were done to further validate the experimental results. The uncertainty calculation was done using the uncertainty calculator in Davis 8.3.1 by LaVision. The uncertainty calculation is based on correlation statistics [36]. The study showed that overall the numerical results agree well with the experimental data and the uncertainty of the PIV measurement is low (below 1% of the pitch line velocity). Figure 4.6 shows the bubble size comparison, Figure 4.7 shows the streamline comparison, and Figure 4.8 shows the PIV measurement uncertainty. More comparisons and discussions of the results can be found in the paper.

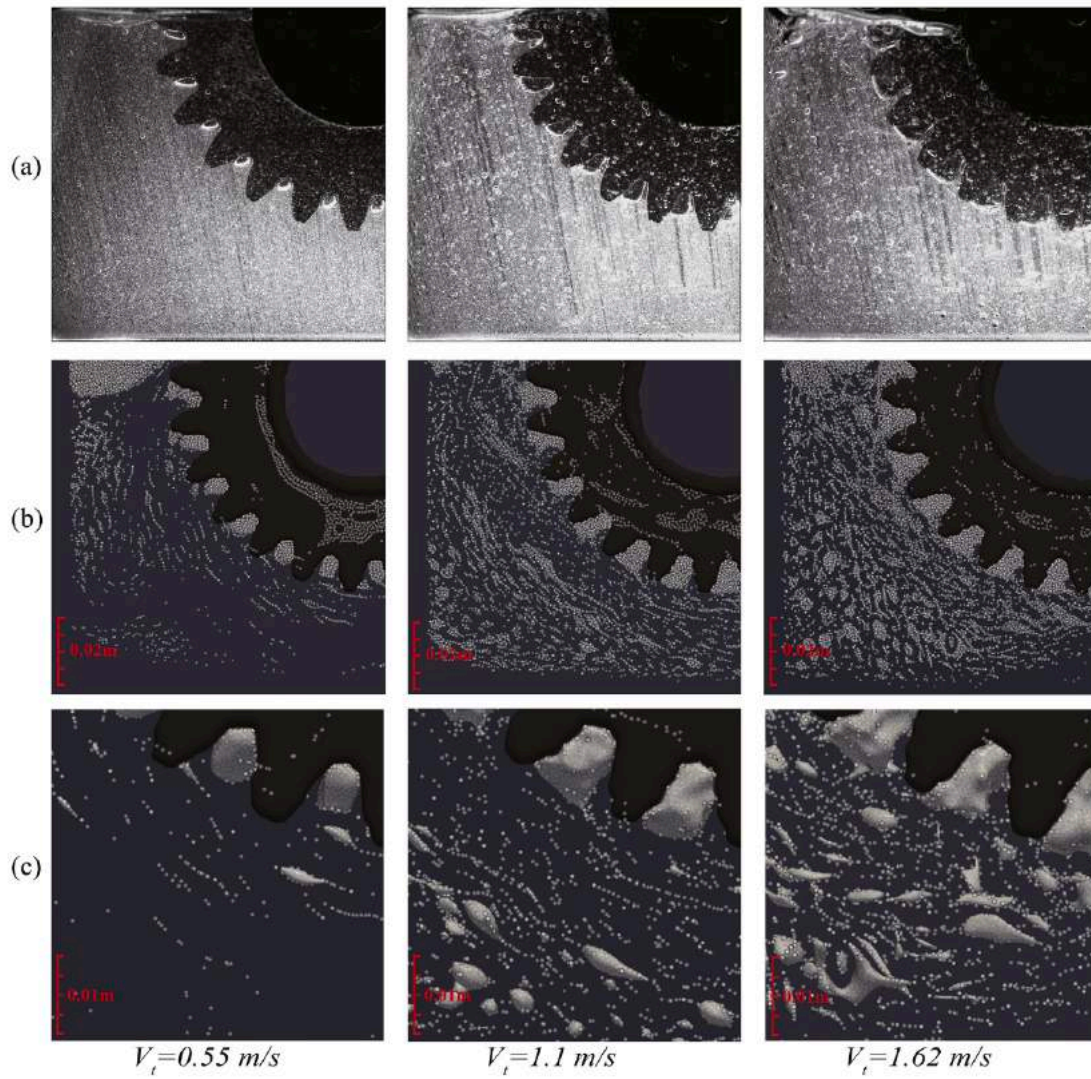


Figure 4.6: The bubble size comparison between PIV and SPH. Row (a) shows experimental images and rows (b) and (c) shows images from SPH

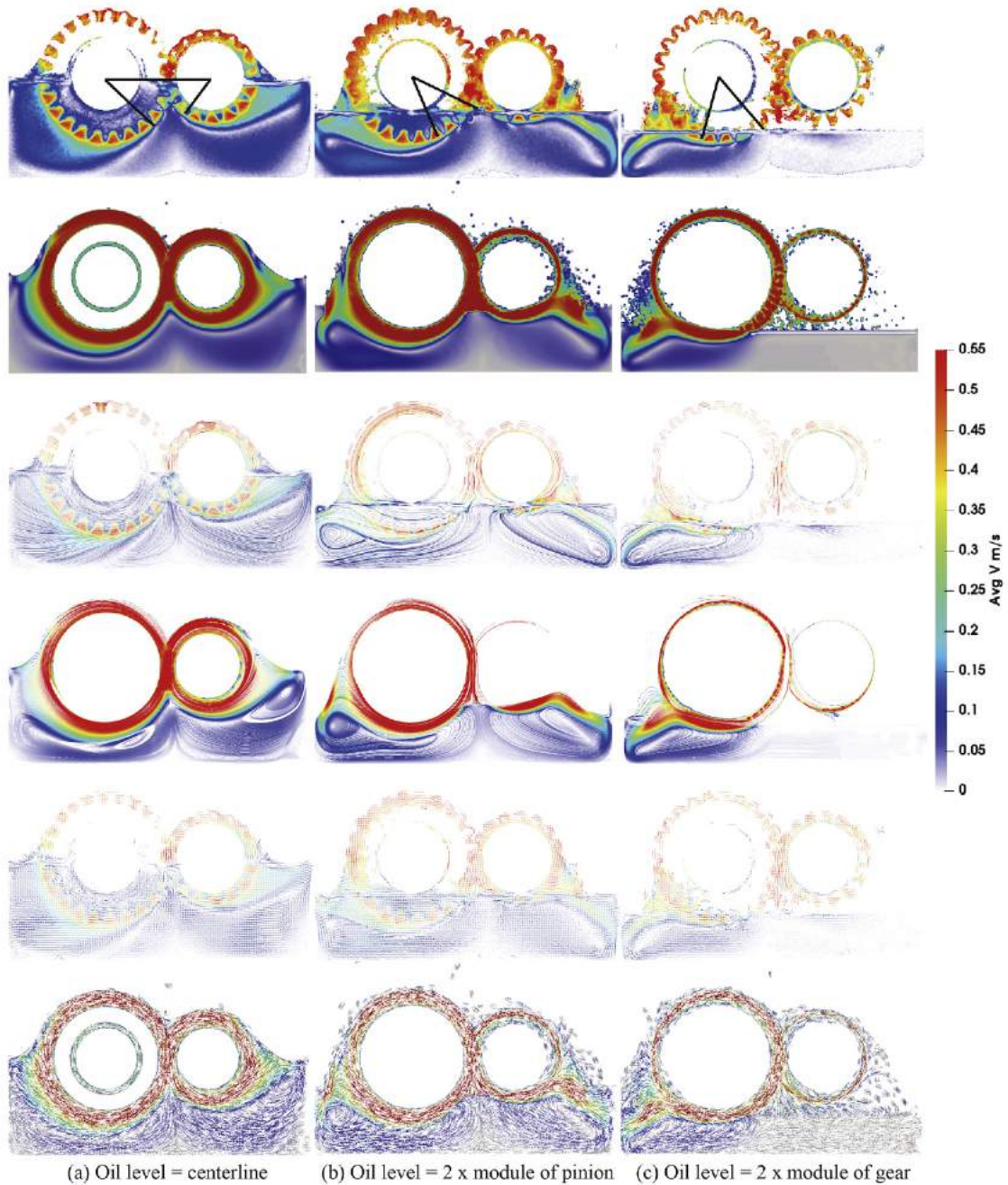


Figure 4.7: The streamline comparison between PIV and SPH. Odd rows show the PIV results and even rows show the SPH results. Test case 0.55 m/s

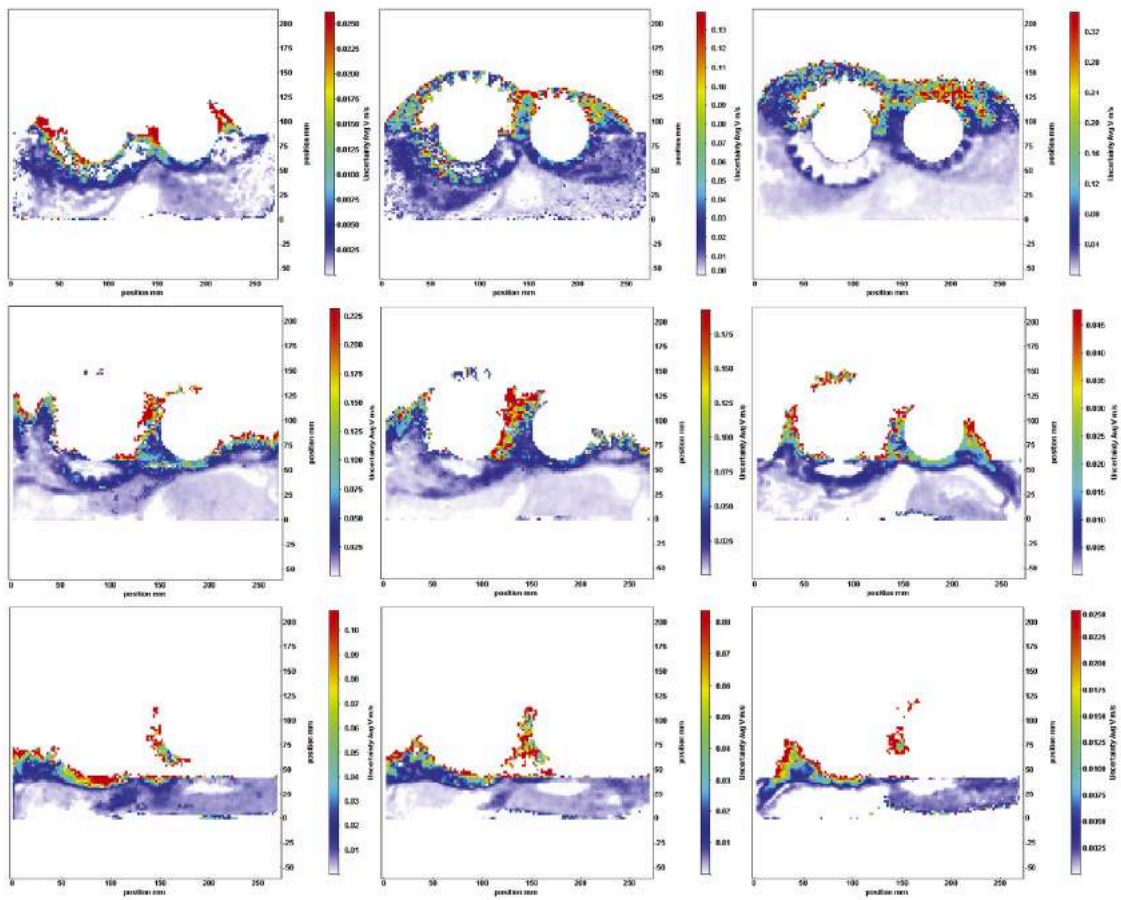


Figure 4.8: The PIV measurement uncertainty

4.4 Paper 4

Guglielmo Minelli, Erwin Adi Hartono, Valery Chernoray, Linus Hjelm, Branislav Basara, and Siniša Krajnović. *Aerodynamic Flow Control for a Generic Truck Cabin Using Synthetic Jets*. *Journal of Wind Engineering and Industrial Aerodynamics*, 168:81-90. September 2017.

Division of work

Guglielmo Minelli designed and built the test rig, performed the measurements and numerical work, post-processed the data, wrote the paper, and presented the paper at the conference. [Erwin Adi Hartono](#) designed and built the test rig, performed the measurements, performed discussion of CFD results, comparison of CFD and experiment, discussion of paper structure and entire paper content, feedback on CFD part and corrections of CFD part, and wrote the experimental part of the paper. Valery Chernoray, Linus Hjelm, and Siniša Krajnović gave feedback and supervised the work.

Summary

For this paper, an experimental study of active flow control in a generic truck cabin model using synthetic jets was conducted. The Reynolds number during the measurement was 5×10^5 . Hot wire anemometry was used to characterise the loudspeaker used in this study to generate synthetic jets as an active flow control actuator. Time-resolved PIV measurements were done at the side and rear of the test object. Results suggest that the chosen frequency of the jets ($F+ = 1, 2.1, 3.1,$ & 6.2) used in this study were able to reduce the size of the separation bubble. The strongest suppression of the separation bubble was found at $F+ = 3.1$. Figure 4.9 shows a comparison of velocity flow fields at the side domain at different actuation frequencies.

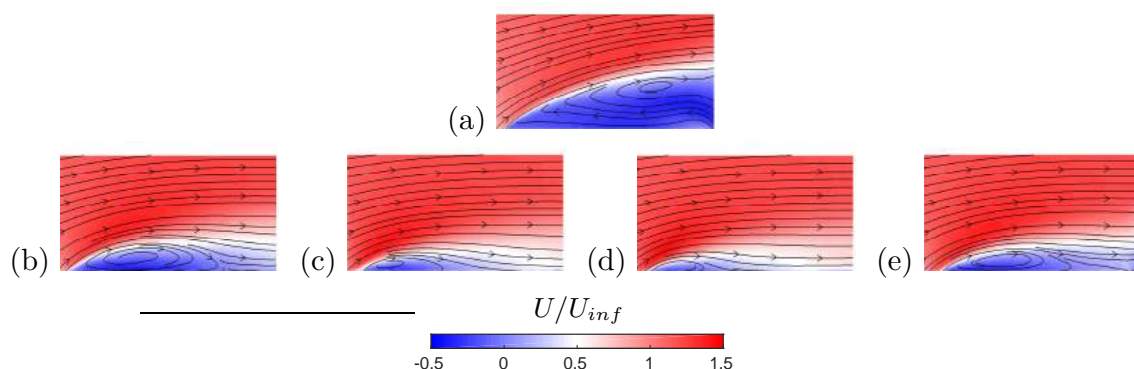


Figure 4.9: PIV result comparison between different actuation cases. (a) no AFC, (b) $F+ = 1$, (c) $F+ = 2.1$, (d) $F+ = 3.1$, and (e) $F+ = 6.2$ [29]

4.5 Paper 5

Guglielmo Minelli, Erwin Adi Hartono, Valery Chernoray, Linus Hjelm, Branislav Basara, and Siniša Krajnović. *Validation of PANS and Active Flow Control for a Generic Truck Cabin*. Journal of Wind Engineering and Industrial Aerodynamics, 171:148-160. December 2017.

Division of work

Guglielmo Minelli designed and built the test rig, performed the measurements and numerical work, post-processed the data, wrote the paper, and presented the paper at the conference. Erwin Adi Hartono designed and built the test rig, performed the measurements, performed discussion of CFD results, comparison of CFD and experiment, discussion of paper structure and entire paper content, feedback on CFD part and corrections of CFD part, and wrote the experimental part of the paper. Valery Chernoray, Linus Hjelm, Branislav Basara, and Siniša Krajnović gave feedback and supervised the work.

Summary

In this paper, the numerical turbulence model PANS with relatively coarse mesh (far beyond LES resolution) was validated with resolved LES and experimental data. The case was separated flow in the A-pillar of a generic truck cabin model. Reynolds number was 5×10^5 . The static pressure on the frontal and side surfaces was compared. The velocity fields, Reynolds stress profile along the recirculation bubble, POD field, and FFT were also compared. Overall results suggest that PANS predicts the flow field quite well despite having a low mesh count compared to the LES and experimental data. Figure 4.10 and Figure 4.11 show a comparison of pressure distribution at the side and rear domains. Figure 4.12 shows a comparison of velocity fields at the side domain. More comparisons and discussion can be found in the paper.

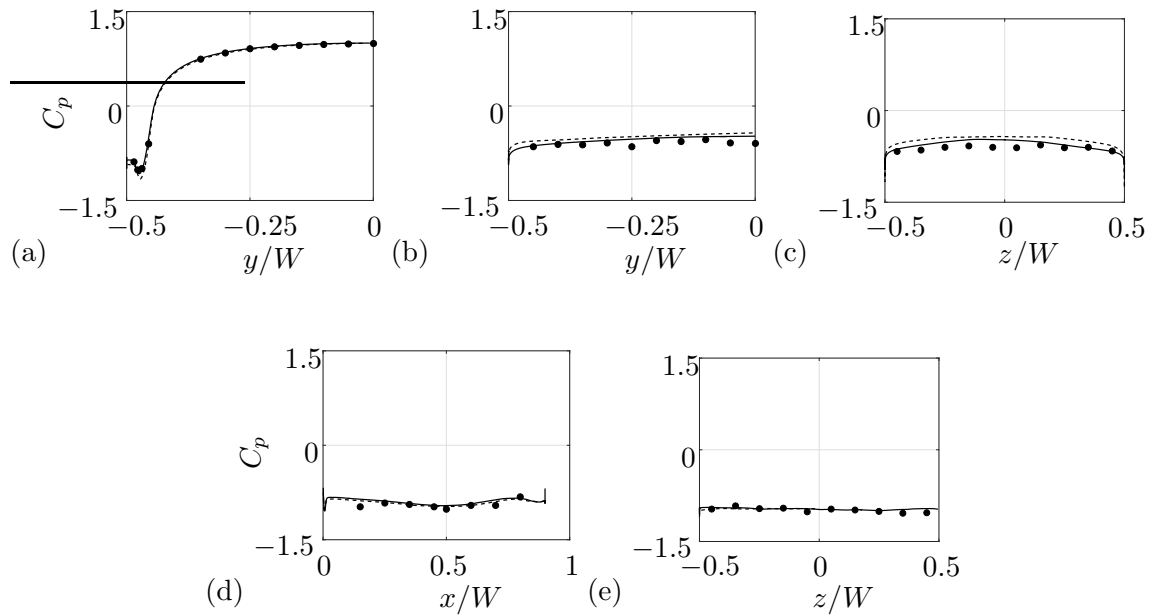


Figure 4.10: Comparison of pressure distribution at the side domain for different numerical methods and experimental data [37]

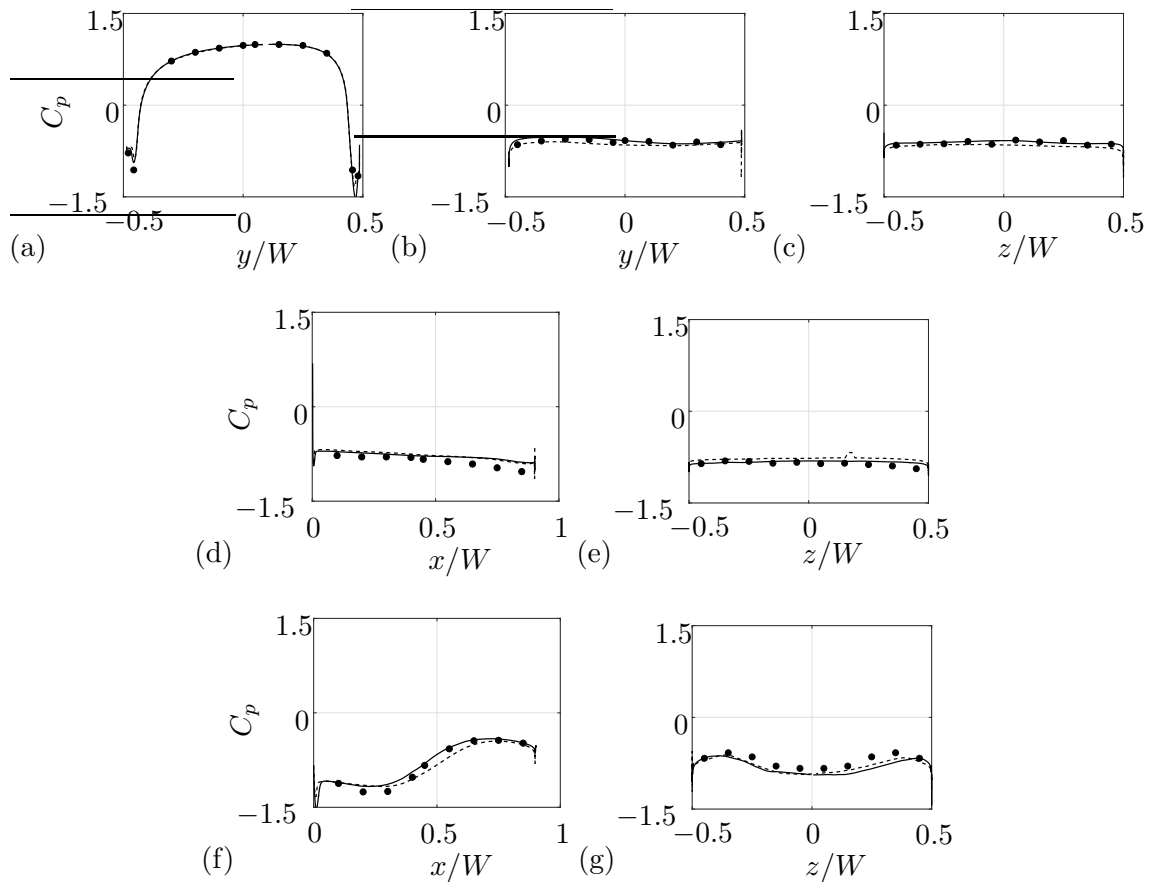


Figure 4.11: Comparison of pressure distribution at the rear domain for different numerical methods and experimental data [37]

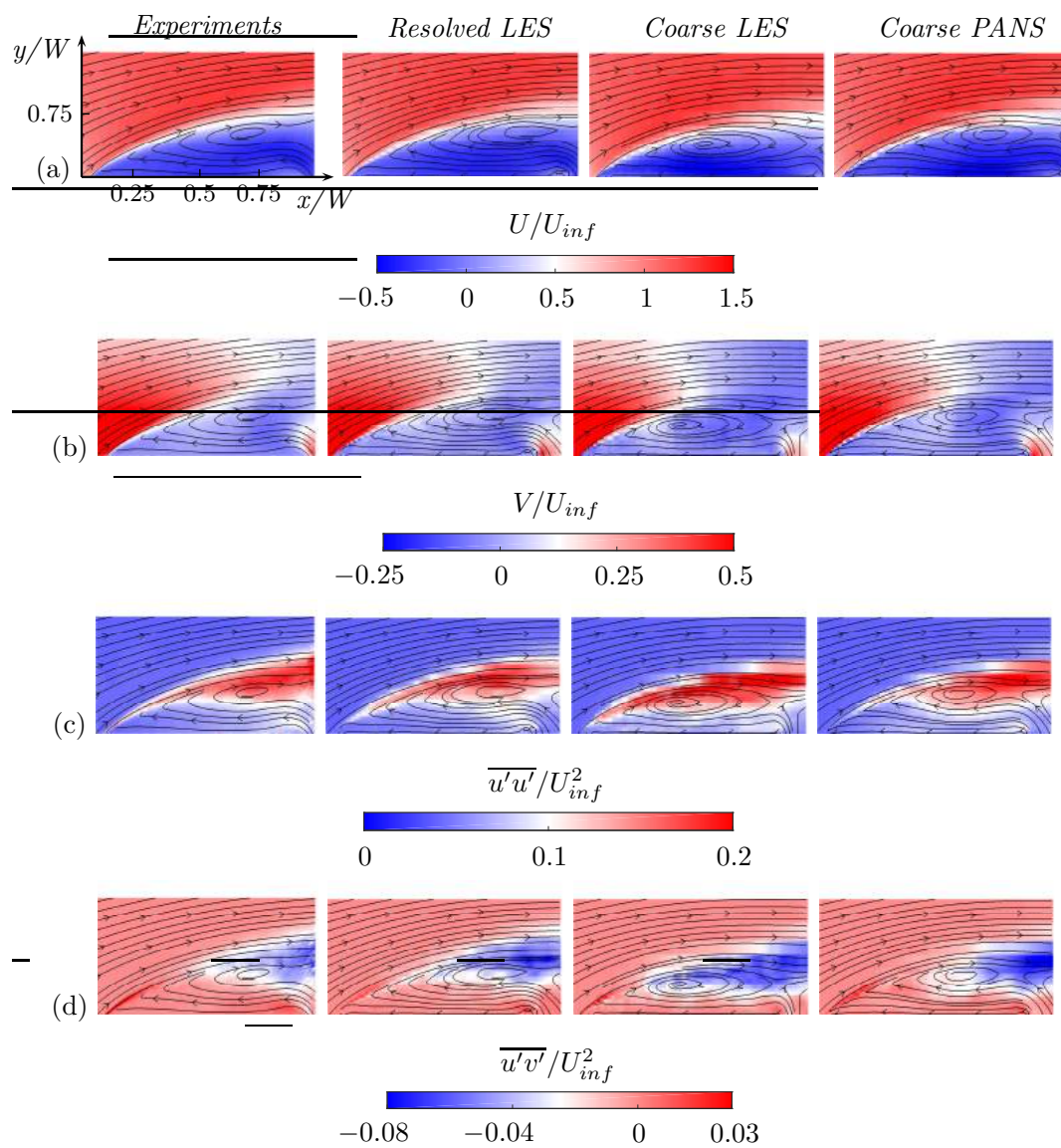


Figure 4.12: Comparison of averaged velocity fields at the side domain for different numerical methods and experimental data [37]

Chapter 5

Unpublished Results on Churning Losses Study

In this chapter there are three things that were studied. Firstly, aeration phenomena inside the transmission was discussed. Secondly, a study to verify a hypothesis that a cylinder with the same outer dimension as a spur gear gives similar fluid flow behaviour inside a transmission. Thirdly, a study to find a general torque loss formula for spur gear with the help of machine learning based on torque measurement data. This chapter provides additional findings on churning losses study. Results of this chapter will be published in additional journal article.

5.1 Aeration

Aeration was observed from the very first tests onward and become a limitation when doing PIV measurements. Aeration is a process where air is entrained and mixed or dissolved in a liquid or substance. Aeration in transmission oil is not desirable. It is believed that aeration can impair the heat transfer inside the transmission. The air bubbles that are generated by the aeration act as an insulator, reducing the heat transfer from the gear to the oil [38]. In terms of energy losses, a study by [39] suggested that aerated oil has additional power losses related to bubble generation and separation. Figure 5.1 shows the visual difference between non-aerated and aerated oil.

Aeration level estimation

The amount of aeration inside the test section was estimated by measuring the froth height and then dividing by the initial oil level height. In this study, the amount of aeration inside the oil is estimated to be 10-20%. Figure 5.2 shows two different aeration levels inside the transmission. Figure 5.2a shows the aeration for a single gear inside a transmission. The froth height was estimated to be 9 mm. The initial oil level was 90 mm. This translates to a 10% aeration level. Figure 5.2b shows the aeration for a pair of cylinders inside a transmission. The froth height was estimated

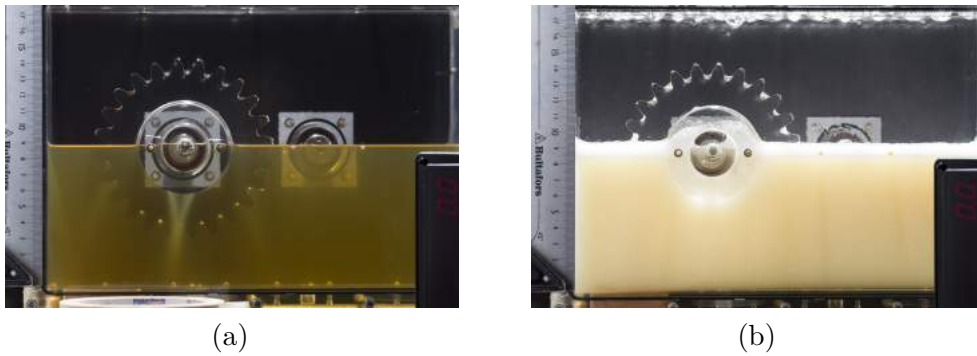


Figure 5.1: Visual difference between non-aerated (a) and aerated oil (b)

to be 20 mm. The initial oil level was 90 mm. This translates to a 20% aeration level.

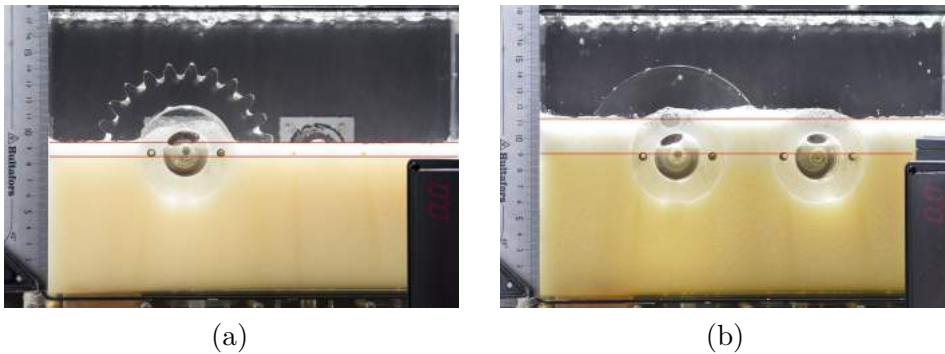


Figure 5.2: Estimation of aeration level inside the transmission. Aeration due to single gear (a) and due to a pair of cylinders (b).

Aeration due to solid impingement

Observation from slow motion footage showed that aeration occurs inside the transmission due to two reasons. The first reason is due to the gear teeth entering the oil sump, as will be discussed in this section. The second reason is due to the oil impinging on the free surface. This will be discussed in section 5.1

Figure 5.3 shows the development of the air bubbles and splash inside a transmission as the gear moves downwards, entering the free surface, and upwards, leaving the free surface. As the gear rotates and enters the free surface, a cavity is created by the gear teeth (Figure 5.3a). Air is drawn into the cavity and trapped inside as the combined force of hydrodynamic pressure, surface tension, and aerodynamic pressure closes the cavity [40]. An air bubble is generated (Figure 5.3b). The buoyancy force lifts the air bubbles upwards and the centrifugal force pushes the air bubbles radially outward. These two forces stretch and divide the air bubble when the forces are large enough to overcome the surface tension (Figure 5.3c). The air bubbles continue to divide until an equilibrium is reached between the forces. Some of the air bubbles are trapped in between the gear teeth and follow the gear teeth rotation. The other are circulated in the recirculation flow (Figure 5.3d-h).

Figure 5.3i-p shows the non-immersed side of the gear. As the gear rotates, the oil is brought upwards by the gear teeth due to the no-slip condition and centrifugal force. There is no bubble generation during the upward movement since no cavity creation occurs in the oil sump. However, air can entrain to the oil bath when the dragged oil falls back into the free surface, as will be explained in the next section.

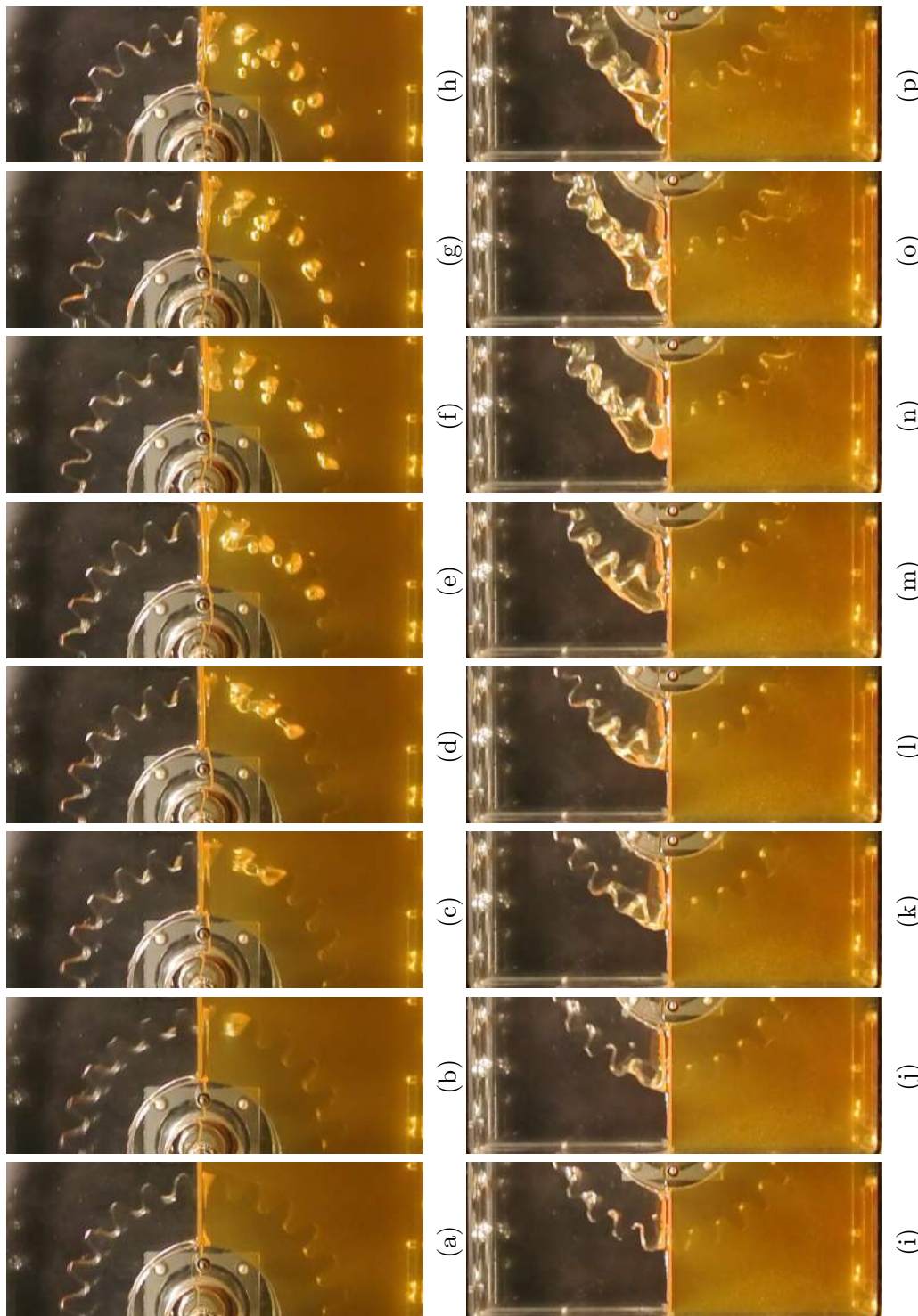


Figure 5.3: Air entrainment to the oil sump at 96 RPM. Note: images are approximately 1 tooth length apart. Figure a-h shows the downward side and Figure i-p shows the corresponding upward side of the gear

Aeration due to liquid impingement

The second reason for aeration inside a gearbox is due to liquid impingement on the free surface. In this study, the phenomenon was observed on a single gear rotating inside a transmission at 250 RPM. At this rotational speed, the oil was mostly being dragged by the gear wheel. As a result, an oil stream was created on top of the gear wheel. The oil stream was then flung into the oil sump, impinging on the free surface. The impingement of liquid draws the air and bubbles are generated ([41] and [42]). Figure 5.4 shows the development of the air bubbles caused by the oil stream entering the free surface of the oil sump inside the transmission.

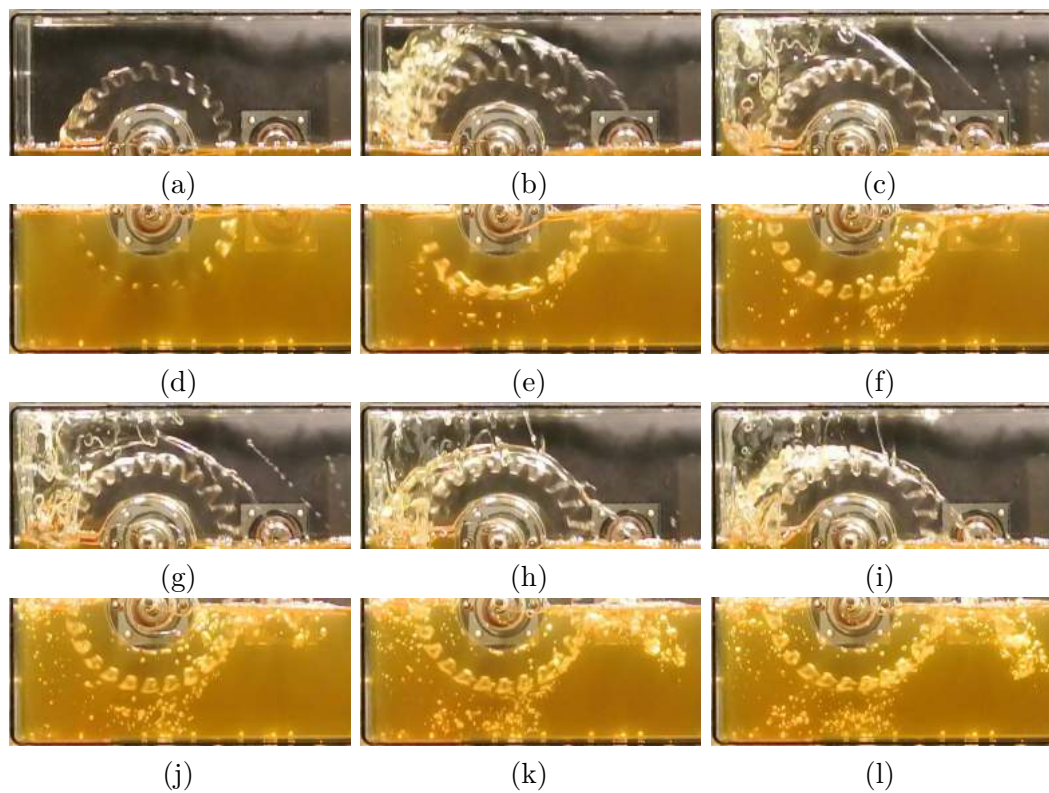


Figure 5.4: Flung oil impinging to the oil sump at 250 RPM.

Torque measurement of aerated oil

In order to study the effect of aeration on the torque, three low RPM cases (150, 200, 250) were chosen. At these low RPM rates, the aeration inside the oil is considered minor and can be used as a base line. The same measurement was repeated with aerated oil. The aeration was generated by rotating the gears at 3000 RPM for approximately 5 minutes. Figure 5.5 shows the torque measurement data for this experiment. It shows a torque increase of about 5-9% in the aerated oil.

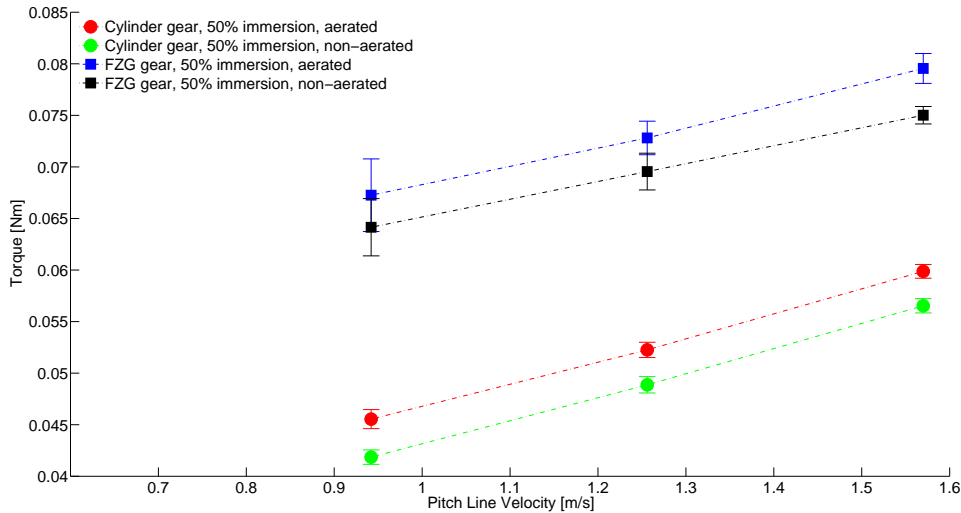


Figure 5.5: Comparison of torque data for the single gear and single cylinder with and without aeration

5.2 Comparison between gear and cylinder with the same outer dimensions

Fluid flow simulation using a finite volume method in a complete transmission is still computationally expensive and unfeasible for some. The main problem is the computational mesh. Solving fluid flow problems numerically using finite volume method requires the computational domain to be discretised into many control volumes (computational mesh). In the case of a gear pair, the cells of the computational mesh in the interlocking area have to be relatively small to be able to resolve the fluid simulation correctly. Several ways to eliminate meshing problems are: to increase the centre distance, to shrink one or both of the gears, to cut gear teeth on one or both gears, and to replace one or both the gears with cylinders [13]. In this study, a gear and a cylinder with the same external geometry were investigated by means of flow visualisation and torque measurement. The results suggested that to a certain degree spur gears can be replaced with a cylinder with the same outer dimensions.

Splash pattern comparison

Figure 5.6 and Figure 5.7 show the quasi-steady splash of the gear and the cylinder rotating solitarily inside a gearbox. The splash pattern above the free surface that was generated by the cylinder was comparable with that of the gear, especially when the comparison was done with a cylinder that rotated 50-100 RPM faster. For example, for the single gear, the splash generated by the gear began to touch the ceiling of the housing at 300 RPM. The splash generated by the cylinder approached the ceiling at 400 RPM.

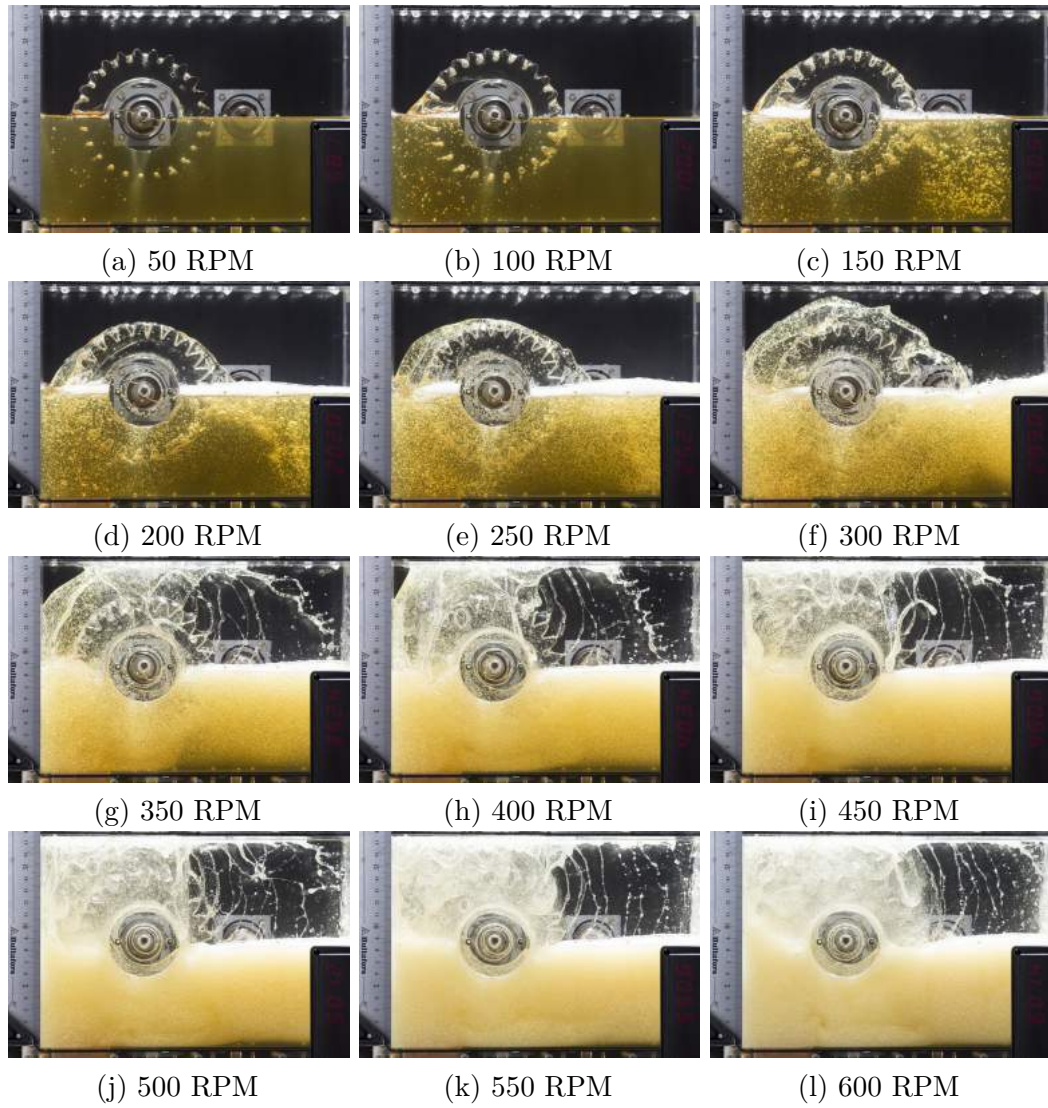


Figure 5.6: Quasi steady flow visualization of a single gear with centreline immersion depth

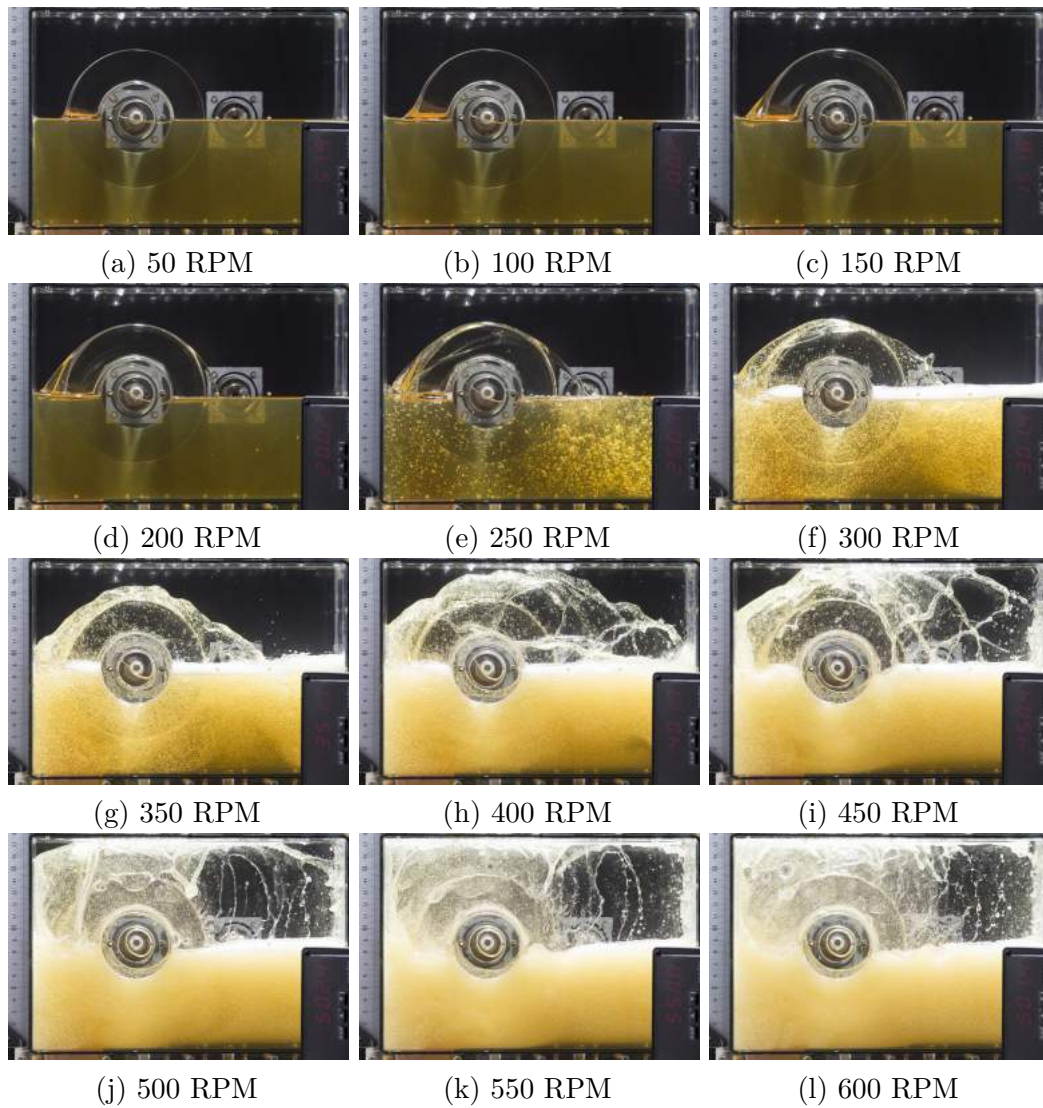


Figure 5.7: Quasi steady flow visualization of a single cylinder with centreline immersion depth

The trapped bubble size comparison

Closer inspection of the area below the free surface indicated that the entrained air was trapped between the gear teeth, and that the size of these trapped bubbles became bigger with additional rotational speed. At about 150 RPM the trapped air occupied the space between the gear teeth. This observation led to the hypothesis that a gear with high enough rotational speed can be replaced by a cylinder provided they have the same outer diameter. Figure 5.8 shows a comparison of the sizes of the bubbles trapped between gear teeth for different rotational speeds.

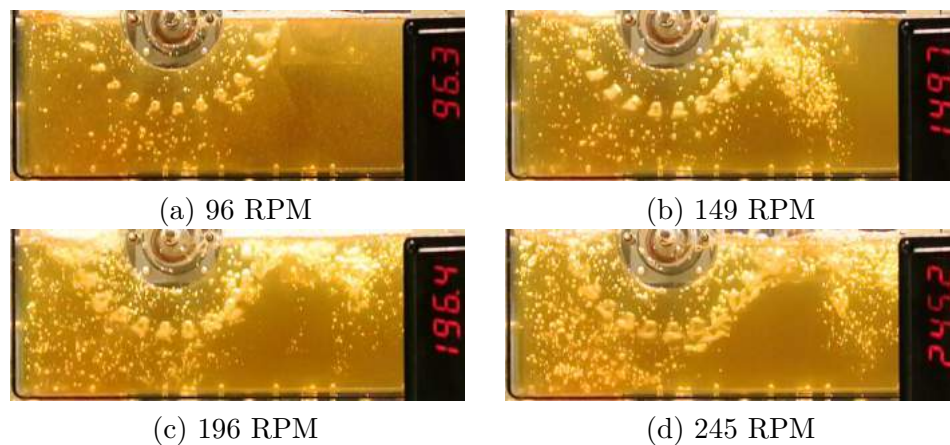


Figure 5.8: Bubble size

The torque measurement comparison

When comparing the same immersion depth, the gear had a higher torque reading compared to the cylinder gear at all pitch line velocities, except at the highest pitch line velocity. At a pitch line velocity of 18.84 m/s, the FZG gear and the cylinder gear with 37.5 and 50% immersion depth resulted in a minor difference in the torque (2%). There were significantly different torques (75% difference) for a 25% immersion depth for the FZG gear and the cylinder gear at the highest pitch line velocity. Although the cylinder gear had the same tip diameter as the FZG gear, the torque results suggest that gear teeth affect torque. Figure 5.9 shows the torques of the single FZG gear and single cylinder gear measurements. It can be seen that the resulting torques from the FZG gear and from the cylinder gear are essentially different.

5.3 Curve fit of torque data using machine learning

In this section, a curve fitting using machine learning was done to estimate the churning losses. Details about machine learning, neural network and biologically inspired optimisation can be found in [43] and [44].

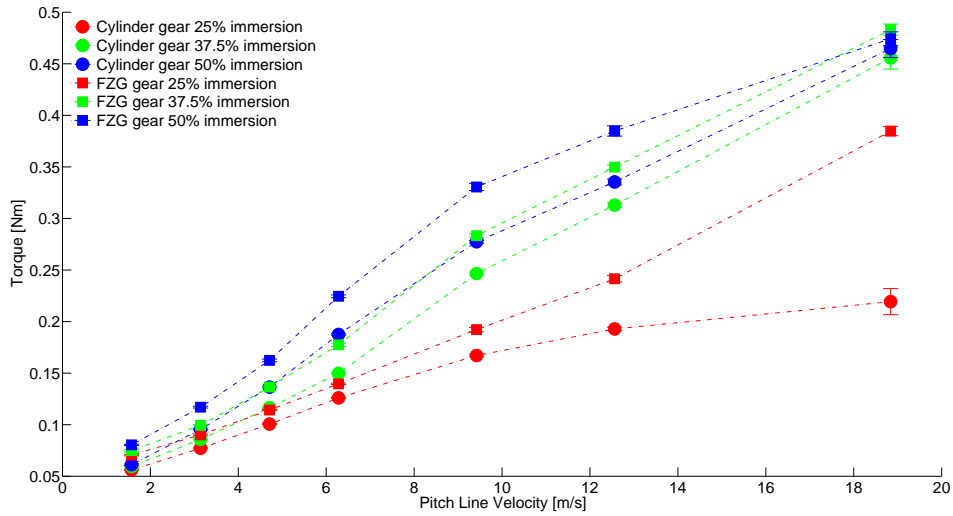


Figure 5.9: Torque of the FZG gear and the cylinder gear with different oil levels and pitch line velocities

The churning loss equation

A study [45] reviewed equations for predicting churning losses from several previous studies on this topic. Figure 5.10 shows a comparison of the churning losses calculated using these equations. The figures show that most of the equations over-predicted the churning losses. The closest to the experimental data is the equation by Changenet.

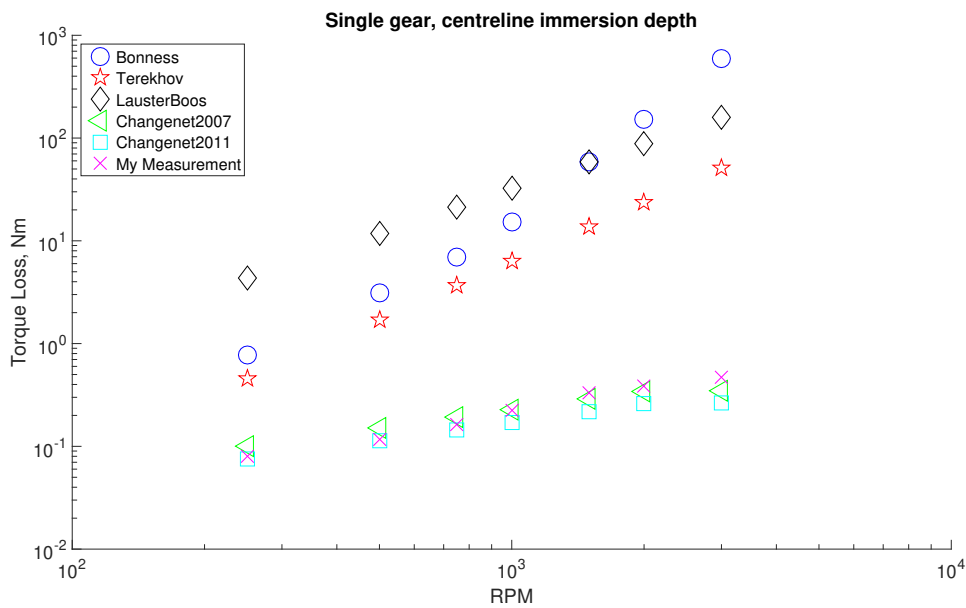


Figure 5.10: Comparison of churning loss equations from different previous studies

The artificial neural network curve fit

The churning loss equation from [20] is the following:

$$C_m = \psi_1(h/D_p)^{\psi_2}(V_o/D_p^3)^{\psi_3}(Fr)^{\psi_4}(Rec)^{\psi_5}(b/R_p)^{\psi_6} \quad (5.1)$$

In this study, machine learning was used to find the exponents (ψ_{1-6}) of Equation 5.1. The programming language used was Python 3.5 with a tensor flow package. The optimisation algorithm was gradient descent. The initial guess was 0.1 for all the exponents (ψ_{1-6}), the learning rate was 0.0001, and the number of iterations was 1000000. For the single cylinder case with 25% immersion depth, the learning rate of 0.001 gave a better fit. The torque measurement data was from a previous study [46]. Figure 5.11 shows a comparison between the equation in [47], [20], and the experimental data. It can be observed that the equation from paper [47] under-predicts the churning losses at rotational speeds above 500 RPM.

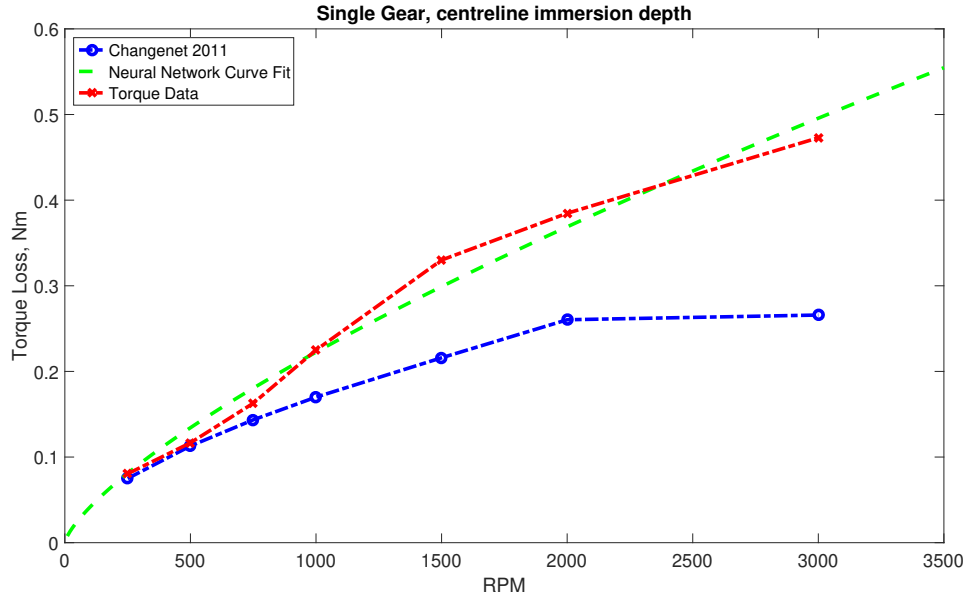


Figure 5.11: Comparison of churning losses equation for single gear with centreline immersion depth

The machine learning algorithm in this study can calculate the exponents relatively quickly. This means that the extension of this study is straightforward and can be applied to many other experimental datasets for a single rotating gear or cylinder partially immersed in oil. Table 5.1 shows the exponents of the equation from different case studies. Figure 5.12 shows the curve fit from single gear and cylinder case studies with different immersion depths.

Case	ψ_1	ψ_2	ψ_3	ψ_4	ψ_5	ψ_6
Single gear 50% immersion	0.317	0.075	0.101	-0.618	-0.035	0.045
Single gear 37.5% immersion	0.285	0.07	0.095	-0.546	-0.036	0.054
Single gear 25% immersion	0.348	0.071	0.083	-0.575	0.075	0.024
Single cylinder 50% immersion	0.266	0.087	0.101	-0.530	-0.092	0.068
Single cylinder 37.5% immersion	0.256	0.092	0.097	-0.491	-0.073	0.069
Single cylinder 25% immersion	0.478	0.043	0.068	-0.846	0.237	-0.048
Single pinion 50% immersion	0.403	0.049	0.191	-0.753	0.084	0.028

Table 5.1: List of coefficients from neural network curve fit for different cases.

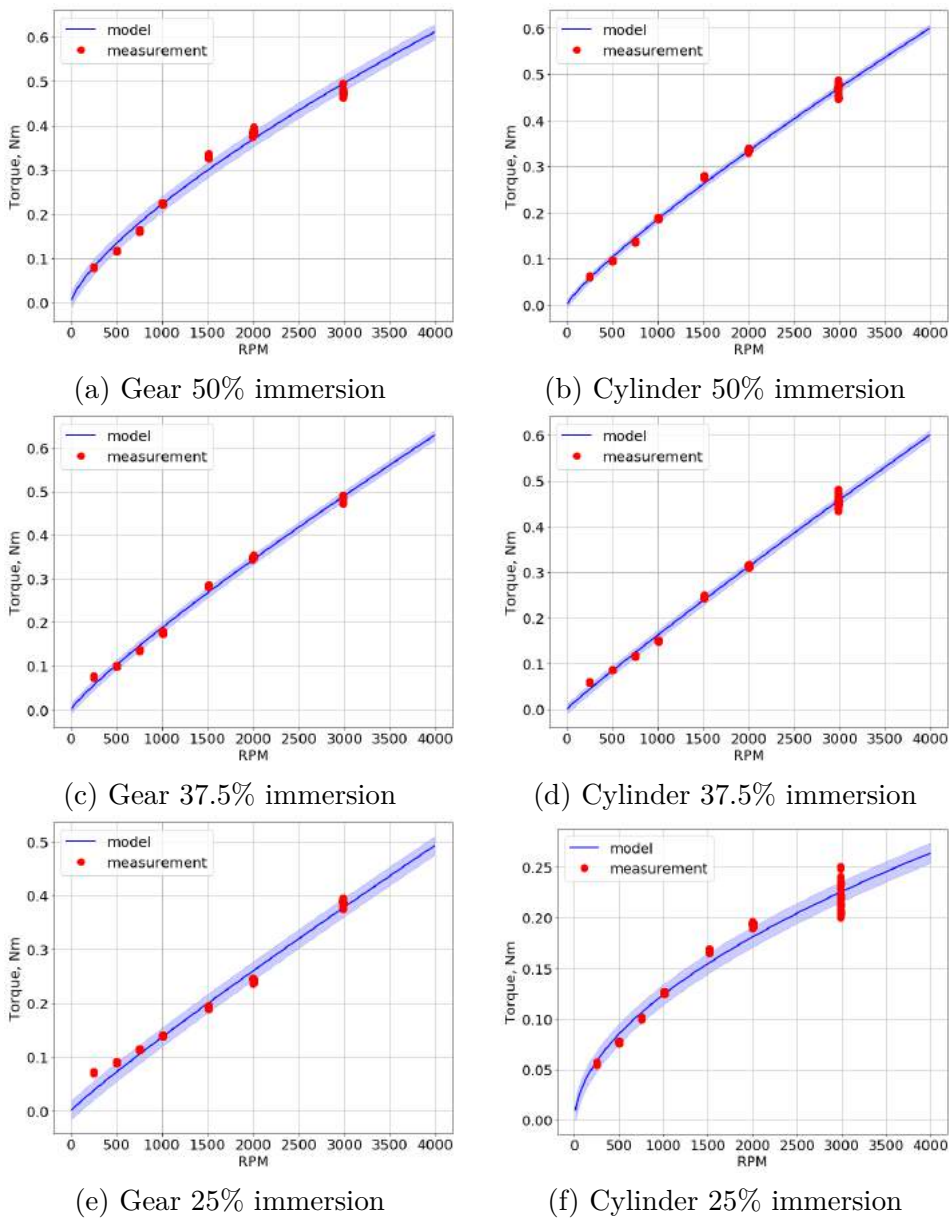


Figure 5.12: Curve fit for different cases

Chapter 6

Concluding Remarks

6.1 Conclusion

In short, both the churning losses and active flow control experimental data that were gathered in this study have added knowledge to the fields of fluid dynamics and have proven to be a valuable resource for the validation and verification of the numerical simulations.

6.1.1 Churning losses inside a transmission

Flow visualisation, velocity measurement, torque measurement, and numerical simulation were performed successfully to study the oil flow around a pair of spur gears inside a transmission. Quasi-steady flow distribution, splash pattern, and aeration mechanisms were studied using flash photography and high speed recording. Recirculation region, vortices, and overall velocity flow field were revealed and measured using PIV. Torque data for different configurations of gear pairs was gathered. A fast and easy curve fit method using a machine learning algorithm was developed in an attempt to generalise the churning losses. The similarities between a spur gear and a cylinder with the same tip diameter were compared in order to investigate the possibility of simplifying gear geometry for simulation. Overall, qualitative and quantitative comparisons of the experimental data and the numerical simulation agree quite well.

6.1.2 Active flow control

Velocity and pressure measurements on the generic truck cabin with two vertical rounded corners to represent the A-pillar of the truck were successfully obtained. The generic truck cabin was equipped with an active flow control device (in the form of synthetic jets) which was located at the rounded corner of the generic truck cabin. Four different actuation frequencies, based on previous LES simulations, were measured. Hot wire anemometry measurements were done to characterise the speakers, which were used as active flow control devices to produce the synthetic jet. Time-resolved PIV measurements were done at the side and rear side of the test

object to quantify the flow velocity field with and without active flow control. Static pressure measurements along the vertical and horizontal midplanes of the front, side, and rear of the test object were also done at two different yaw configurations, 0° and 10° , to assess the performance of the active flow control. Drag force was estimated using the pressure measurement data. The results suggest that separation was suppressed when active flow control was used. Overall, qualitative and quantitative comparisons between the experimental data and the numerical simulation show good agreement.

6.2 Recommendation for future works

There is always room for improvement. Here are some recommendations for future work to further our knowledge and move closer to real world application. Note that the order of appearance does not translate to the order of importance.

6.2.1 Churning losses inside a transmission

Heat transfer

The present study focuses on oil flow around a pair of spur gears inside a gearbox in order to understand the mechanisms of torque loss due to the presence of oil. It would be interesting for future studies to investigate the impact of the flow on the heat transfer from the gear teeth to the oil and vice versa.

Series of gears in the axial direction

The present study uses a pair of gears partially submerged inside a transmission. It would be of interest for future studies to investigate the flow fields created by a series of gears along the axial axis. This should represent a countershaft in real application.

Helical gears

The present study uses spur gears. It would be interesting for future studies to investigate helical gears, as this geometry is closer to real applications in truck transmissions.

Housing optimisation and flow redirection

The present study uses rectangular-shaped transmission housing. It would be of interest for future studies to find the optimal shape of the housing, i.e. the shape which can give the least torque loss and the most heat transfer with the same volume of oil.

Higher frame rate camera

It may be of interest to use a higher frame rate camera when studying the aeration in more detail and for PIV measurement at higher rotational speeds.

6.2.2 Active flow control

Yaw angle case

Real-world wind direction is seldom parallel to the vehicle direction. Future measurements determining the flow field in yaw configuration with and without active flow controls will be valuable.

Realistic models

More realistic models with side view mirrors and angled front faces would be of interest to implement in future studies.

Different actuators

The synthetic jet in this study was created using a loudspeaker. Different actuators such as plasma or piezo would be of interest to implement in future studies.

Closed loop control

Active flow control has proven to be able to suppress separation in this study. However, the actuation frequency and amplitude are specific to one application only. Future studies which attempt to tune the actuation frequency and amplitude automatically depending on the feedback from the surroundings would be beneficial for real application.

Bibliography

- [1] Earth Science Communications Team at NASA’s Jet Propulsion Laboratory. *A blanket around the Earth*. Ed. by H. Shaftel, R. Jackson, and S. Callery. Aug. 8, 2018. URL: <https://climate.nasa.gov/causes/>.
- [2] European Environment Agency. *Greenhouse gas emissions from transport*. Ed. by D. Vedlugaite. July 11, 2018. URL: <https://www.eea.europa.eu/data-and-maps/indicators/transport-emissions-of-greenhouse-gases/transport-emissions-of-greenhouse-gases-10>.
- [3] K. Holmberg, P. Andersson, N.-O. Nylund, K. Mäkelä, and A. Erdemir. “Global energy consumption due to friction in trucks and buses”. In: *Tribology International* 78 (2014), pp. 94–114. DOI: <https://doi.org/10.1016/j.triboint.2014.05.004>.
- [4] G. Niemann and H. Winter. *Maschinenelemente Band II – Getriebe allgemein, Zahnradgetriebe – Grundlagen, Stirnradgetriebe*. Springer-Verlag, 1983.
- [5] H. Liu, T. Jurkschat, T. Lohner, and K. Stahl. “Detailed Investigations on the Oil Flow in Dip-Lubricated Gearboxes by the Finite Volume CFD Method”. In: *Lubricants* 6.47 (2 2018). ISSN: 20754442. DOI: 10.3390/lubricants6020047.
- [6] M. J. Neale. *The Tribology Handbook*. 2nd ed. Butterworth-Heinemann, 1995. ISBN: 0 7506 1198 7.
- [7] Noria Corporation. *Lubrication Basic*. Aug. 10, 2018. URL: <https://www.machinerylubrication.com/Read/24100/lubrication-basics>.
- [8] B.-R. Höhn, K. Michaelis, and H.-P. Otto. “Influence of Immersion Depth of Dip Lubricated Gears on Power Loss, Bulk Temperature and Scuffing Load Carrying Capacity”. In: *Int J Mech Mater Des* 4 (2008), pp. 145–156.
- [9] T. Moshhammer, F. Mayr, K. Kargl, and C. Honerger. “Simulation of Oil Flow in Gear Box Housing”. In: *Proc. SAE 2006 World Congress and Exhibition*. Apr. 3, 2006. DOI: <https://doi.org/10.4271/2006-01-1574>.
- [10] L. Li, H. K. Versteeg, G. K. Hargrave, T. Potter, and C. Halse. “Numerical Investigation on Fluid Flow of Gear Lubrication”. In: *SAE International Journal of Fuels and Lubricants* 1(1) (2008), pp. 1056–1062.
- [11] C. Gorla, F. Concli, K. Stahl, B.-R. Höhn, K. Michaelis, H. Schultheib, and J.-P. Stemplinger. “Hydraulic Losses of a Gearbox: CFD Analysis and Experiments”. In: *Tribology International* 66 (2013), pp. 337–344.

- [12] D. Saegusa and S. Kawai. “CFD Analysis of Lubricant Fluid Flow in Automotive Transmission”. In: *Proc. SAE 2014 World Congress and Exhibition*. Apr. 1, 2014. DOI: <https://doi.org/10.4271/2014-01-1772>.
- [13] Q. Peng, L. Gui, and Z. Fan. “Numerical and experimental investigation of splashing oil flow in a hypoid gearbox”. In: *Engineering Applications of Computational Fluid Mechanics* 12 (1 Feb. 11, 2018), pp. 324–333. DOI: <https://doi.org/10.1080/19942060.2018.1432506>.
- [14] F. Lemfeld and K. Fraña. “Investigation of Multiphase Flows by High Speed Camera”. In: *Proc. Experimental fluid mechanics 2009 Liberec (Czech Republic)*. 2009.
- [15] Z. Várhegyi and G. Kristóf. “Mass Flux Distribution Measurements and Visualizations of a Fluid Sheet Generated by a Partially Immersed Dip-Lubricated Gear”. In: *Periodica Polytechnica Mechanical Engineering* 60(2) (Mar. 9, 2016), pp. 66–81. DOI: <https://doi.org/10.3311/PPme.7764>.
- [16] V. Chernoray and M. Jahanmiri. “Experimental Study of Multiphase Flow in a Model Gearbox”. In: *WIT Transactions on Engineering Sciences* 70 (2011), pp. 153–164. ISSN: 1743-3533. DOI: 10.2495/MPF110131.
- [17] H.-P. Otto. “Flank Load Carrying Capacity and Power Loss Reduction by Minimised Lubrication”. Doctoral Thesis. Technical University of Munich, Jan. 9, 2009.
- [18] P. Luke and A. V. Olver. “A Study of Churning Losses in Dip-Lubricated Spur Gears”. In: *Proc. Instn. Mech. Engrs* 213 Part G (Aug. 10, 2012), pp. 337–346.
- [19] S. Seetharaman, A. Kahraman, M. D. Moorhead, and T. T. Petry-Johnson. “Oil Churning Power Losses of a Gear Pair: Experiments and Model Validation”. In: *Journal of Tribology* 131 (2009), pp. 022202-1–022202-10. DOI: 10.1115/1.3085942.
- [20] C. Changenet, G. Leprince, F. Ville, and P. Velez. “A Note on Flow Regimes and Churning Loss Modeling”. In: *J. Mech. Des* 133 (12 Dec. 9, 2011), pp. 1–5. DOI: 10.1115/1.4005330.
- [21] K. Cooper. “Bluff Body Drag Manipulation Using Pulsed Jets and Coanda Effect”. In: *Journal of Fluid Mechanics* 805 (2016), pp. 422–459.
- [22] K. Cooper. “Truck Aerodynamics Reborn - Lessons from the Past”. In: *SAE Transactions Journal of Commercial Vehicle* 112 (2003), pp. 132–142.
- [23] T. Duriez, S. L. Brunton, and B. R. Noack. *Machine Learning Control – Taming Nonlinear Dynamics and Turbulence*. Springer, 2017. ISBN: 978-3-319-40624-4. DOI: 10.1007/978-3-319-40624-4.
- [24] D. You and P. Moin. “Active Control of Flow Separation over an Airfoil using Synthetic Jets”. In: *Journal of Fluids and Structure* 24 (2008), pp. 1349–1357.
- [25] DIN ISO 14635-1. *Gears - FZG test procedure - Part 1: FZG gear test method A/8,3/90 for relative load carrying capacity of oils*. Standard. International Organization for Standardization, 2000.

- [26] NYNAS. *Product Data Sheet Nytex 810*. Aug. 3, 2018. URL: [https://nyport.nynas.com/Apps/1112.nsf/%20wnpds/Nytex_810_ASTM/\\$File/PDS_Nytex_810_EN.pdf](https://nyport.nynas.com/Apps/1112.nsf/%20wnpds/Nytex_810_ASTM/$File/PDS_Nytex_810_EN.pdf).
- [27] P. Freymuth. “Flow Visualization in Fluid Mechanics”. In: *Rev. Sci. Instrum.* 64 (1) (1993).
- [28] Nikon. *Autofocus Speedlight SB-700 User’s Manual*. Aug. 3, 2018. URL: <https://cdn-10.nikon-cdn.com/pdf/manuals/Speedlights/SB-700.pdf>.
- [29] G. Minelli, E. A. Hartono, V. Chernoray, L. Hjelm, B. Basara, and S. Krajnović. “Aerodynamic Flow Control for a Generic Truck Cabin Using Synthetic Jets”. In: *Journal of Wind Engineering and Industrial Aerodynamics* 168 (2017), pp. 81–90.
- [30] C. Tropea, A. Yarin, and J. F. Foss. *Springer Handbook of Experimental Fluid Mechanics*. Springer-Verlag Berlin Heidelberg, 2007. ISBN: 978-3-540-30299-5.
- [31] R. J. Adrian and J. Westerweel. *Particle Image Velocimetry*. Cambridge, 2011. ISBN: 978-0-521-44008-0.
- [32] M. Raffel, C. E. Willert, F. Scarano, C. J. Kähler, S. T. Wereley, and J. Kompenhans. *Particle Image Velocimetry - A Practical Guide*. Springer, 2018. ISBN: 978-3-319-68852-7. DOI: <https://doi-org.proxy.lib.chalmers.se/10.1007/978-3-319-68852-7>.
- [33] E. A. Hartono, M. Golubev, and V. Chernoray. “PIV Study of Fluid Flow Inside a Gearbox”. In: *Proc. 10th International Symposium on Particle Image Velocimetry - PIV13*. 2013.
- [34] E. A. Hartono, A. Pavlenko, and V. Chernoray. “Stereo-PIV Study of Oil Flow inside a Model Gearbox”. In: *Proc. 17th International Symposium on Applications of Laser Techniques to Fluid Mechanics*. 2014.
- [35] Dantec Dynamics. *FPP, Fluorescent Polymer Particles*. Aug. 7, 2018. URL: <https://www.dantecdynamics.com/fpp-fluorescent-polymer-particles>.
- [36] B. Wieneke. “PIV Uncertainty Quantification from Correlation Statistics”. In: *Journal of Meas. Sci. Technol* 26.7 (2015).
- [37] G. Minelli, E. A. Hartono, V. Chernoray, L. Hjelm, B. Basara, and S. Krajnović. “Validation of PANS and Active Flow Control for a Generic Truck Cabin”. In: *Journal of Wind Engineering and Industrial Aerodynamics* 171 (2017), pp. 148–160.
- [38] J. Fitch. “The Perils of Aerated Oil - Let Your Machine Burp”. In: *Practicing Oil Analysis* 1 (2005).
- [39] G. LePrince, C. Changenet, F. Ville, P. Vexex, C. Dufau, and F. Jarnias. “Influence of Aerated Lubricants on Gear Churning Losses—An Engineering Model”. In: *Tribology Transactions* 54 (2011), pp. 929–938. DOI: <https://doi.org/10.1080/10402004.2011.597542>.
- [40] J. M. Aristoff and J. W. M. Bush. “Water entry of small hydrophobic spheres”. In: *J. Fluid Mech.* 619 (2009), pp. 45–78. DOI: [10.1017/S0022112008004382](https://doi.org/10.1017/S0022112008004382).

-
- [41] W. K. Soh et al. “The Entrainment of Air by Water Jet Impinging on A Free Surface”. In: *Experiments in Fluids* 39 (2005), pp. 496–504.
- [42] X. Qu et al. “Experimental Characterization of air-entrainment in a plunging jet”. In: *Experimental Thermal and Fluid Science* 44 (2012), pp. 51–61.
- [43] C. M. Bishop. *Pattern Recognition and Machine Learning*. Springer, 2006. ISBN: 978-0387-31073-2.
- [44] M. Wahde. *Biologically Inspired Optimization Methods - An Introduction*. WIT Press, 2008. ISBN: 978-1-84564-148-1.
- [45] V. Stavytskyy, P. Nosko, P. Fil, A. Karpov, and N. Velychko. “Load-Independent Power Losses of Gear Systems: A Review”. In: *TEKA Kom. Mot. i Energ. Roln.* 10B (2010), pp. 205–213.
- [46] E. A. Hartono. “Study of fluid flow inside a gearbox”. Licentiate Thesis. Chalmers University of Technology, Oct. 14, 2014.
- [47] C. Changenet and P. Velex. “A Model for the Prediction of Churning Losses in Geared Transmissions - Preliminary Results”. In: *J. Mech. Des* 129 (1 2007), pp. 128–133. DOI: 10.1115/1.2403727.